IOP Publishing | International Atomic Energy Agency Nuclear Fusion

Nucl. Fusion **59** (2019) 096023 (18pp) https://doi.org/10.1088/1741-4326/ab233a

Robust nonlinear burn control in ITER to handle uncertainties in the fuel-line concentrations

Andres Pajares and Eugenio Schuster

Department of Mechanical Engineering and Mechanics, Lehigh University, Bethlehem, PA 18015, United States of America

E-mail: andres.pajares@lehigh.edu

Received 20 December 2018, revised 26 April 2019
Accepted for publication 17 May 2019
Published 30 July 2019

Abstract

Tight regulation of the burn condition in ITER has been proven possible in simulations by the use of robustification techniques even under emulated time-dependent variations in the fuel concentration. One of the most fundamental control problems arising in ITER and future burning-plasma tokamaks is the regulation of the plasma temperature and density to produce a determined amount of fusion power while avoiding possible thermal instabilities. Such problem, known as burn control, requires the development of controllers that integrate all the available actuators. Moreover, the complex burning-plasma dynamics and the uncertain nature of some of its components suggest that nonlinear, robust, burn controllers are necessary. For instance, the deuterium–tritium concentration in the fueling lines may vary over time and the estimation of such variation during operation may be difficult or not even possible. Available actuators for the regulation of the burn condition are auxiliary power modulation, fueling rate modulation, and impurity injection. Also, recent experiments in the DIII-D tokamak have shown that in-vessel coil-current modulation can be used for burn control purposes. The in-vessel coils generate non-axisymmetric magnetic fields that have the capability to decrease the plasma-energy confinement time, which allows for regulation of the plasma energy during positive energy perturbations. In this work, all these actuators are used to design a nonlinear burn controller which is robust to unknown variations in the deuterium–tritium concentration of the fueling lines. Furthermore, fueling rate modulation is not only used to control the plasma density, but also to control the plasma energy, if necessary, by means of isotopic fuel tailoring. The model-based nonlinear controller is synthesized from a zero-dimensional model of the burning-plasma dynamics. A nonlinear simulation study is carried out to illustrate the successful controller performance in ITER-like scenarios in which unknown variations of the deuterium–tritium concentration of the fueling lines are emulated.

Keywords: burn control, plasma control, nonlinear control, robust control

(Some figures may appear in colour only in the online journal)

1. Introduction

For tokamaks to be commercially competitive, stable operation for long periods of time with a large Q value will be necessary, where Q is the ratio between the generated fusion power and the injected auxiliary power. To achieve such performance, precise control of the plasma temperature and density is required, as these variables determine the fusion power. This problem, known as burn control, requires control algorithms with the capability of regulating the plasma temperature and density to produce a determined amount of fusion power while preventing thermal instabilities.

Traditional actuators considered for burn control in tokamaks include auxiliary power modulation [1, 2], fueling

 © 2019 IAEA, Vienna Printed in the UK

rate modulation [3, 4], and controlled impurity injection [5, 6]. An additional actuator that might be considered is in-vessel coil-current modulation. Recent experiments in the DIII-D tokamak suggested the possibility of using the in-vessel coils for burn control purposes [7]. When electric current is driven through the in-vessel coils, these generate non-axisymmetric magnetic fields that modify the magnetic configuration of the tokamak. In [7], the capability of the in-vessel coils to modify the plasma-energy confinement time and control the plasma energy is shown in low collisionality, low density discharges. Reductions in the plasma-energy confinement time were observed after activation of the in-vessel coils, together with decreases in the pedestal electron density. Changes in the plasma shape and edge-localized mode activity were small after application of non-axisymmetric magnetic fields. Other previous experiments in DIII-D [8], TEXT [9] and Tore Supra [10] also showed a degradation in confinement and/or electron density reduction after application of non-axisymmetric magnetic fields. However, in discharges with higher plasma collisionality and higher density in DIII-D, no reductions in the plasma-energy confinement time or pedestal electron density were found [8]. Although the effects of non-axisymmetric fields on confinement degradation are still under study, it is reasonable to include in-vessel coil-current modulation as a potential actuator for burn control in low collisionality plasmas as the ones expected in ITER [11].

In ITER, two fueling techniques will be considered: gas puffing and pellet injection. Present-day tokamaks normally use gas puffing as the primary fueling technique. However, in future tokamaks working at higher densities and high-confinement regimes, gas puffing is predicted to have a poor fueling efficiency due to the existence of a high plasma-edge pressure gradient [12]. Therefore, techniques like pellet injection, that has a higher capability to penetrate the magnetic fields and deposit particles into the plasma core, will most likely be the primary fueling technique in ITER. Gas puffing will mainly be used to fuel the plasma edge in order to enhance impurity transport out of the plasma core and keep optimal divertor conditions [12]. Two pellet injectors will be available in the initial phase of ITER. Each of these pellet injectors will be able to produce pellets made of both deuterium (D) and tritium (T), with a concentration of up to 90% T. One of the pellet injectors will be used to inject pellets made of only D, while the other pellet injector will inject pellets with the highest possible concentration of T. In this work, the first pellet injector is denoted as D pellet injector, whereas the second pellet injector is denoted as D–T pellet injector. Although the nominal concentrations for these lines are 100% D and 10%D–90%T, respectively, the D–T concentration of those pellets may vary over time. This is mainly due to the fact that T tends to permeate very easily through the plasma facing components (PFCs), and also through the tritium exhaust and re-processing system [13]. Most PFCs will be made of beryllium (like the vacuum vessel walls), tungsten (divertor components) or carbon, whereas the tritium exhaust and re-processing systems will include materials such as ceramics, different kinds of steel, and aluminum alloys. The T permeability and solubility in all these materials is variable, so part of the T will inevitably diffuse into the materials which are more susceptible at a rate which will be difficult to estimate during operation. As a result, keeping a constant D–T concentration in the pellets may be just not possible. These concentration variations, which may be in turn hard or impossible to measure in real time, can decrease the burning plasma performance to unacceptable levels. Therefore, burn controllers that are robust to unknown variations in the D–T concentrations will be required for successful, accurate control in future burning-plasma tokamaks.

In the past, the most common approach to model-based burn control was to use linear control techniques after approximately linearizing the nonlinear models for the burning-plasma dynamics. However, an effective burn controller must be capable of not only regulating the system stably around a desired operating point (around which the model linearization is carried out) but also driving the system into or out of the burning plasma mode and from one operating point to another within the burning plasma mode (e.g. different Q or fusion power). Therefore, the complex nonlinear physics that characterizes the burning plasma dynamics dictates that controllers that embed the nonlinear dynamic models in the control synthesis process will have an improved performance when compared to those controllers that only use approximate linear models. In order to overcome the operability limits imposed by the linearization of the burn dynamics, our present and prior work is characterized by the use of nonlinear techniques for burn control. In [14], a model-based nonlinear controller was introduced for the first time to regulate the burn condition by combining auxiliary power modulation, fueling rate modulation, and impurity injection. A different approach to fueling rate modulation was introduced in [15] to control the mix of deuterium and tritium by using the so-called isotopic fuel tailoring approach [16], which allows for reducing the generated fusion power and, therefore, controlling the plasma energy. More recently, in-vessel coil-current modulation was included in the control design in conjunction with isotopic fuel tailoring [17].

In this work, a nonlinear, model-based controller is first synthesized by using Lyapunov-based control-design techniques. The proposed controller integrates all the actuators available for burn control: auxiliary power modulation, in-vessel coil-current modulation, fueling rate modulation, and controlled impurity injection. The control algorithm considers that the primary methods to regulate the plasma energy are auxiliary power modulation and in-vessel coil-current modulation. Fueling rate modulation is used in isotopic fueling mode to control the plasma energy and total density if both the auxiliary power and the in-vessel coil current saturate, or if the total plasma density, n, is such that $n > 2f_{GW}n_{GW}$, where $0 < f_{GW} \leqslant 1$ is a design parameter, and n_{GW} is the Greenwald density limit. Otherwise, fueling rate modulation is exclusively used to control the D and T densities. Reduction of the plasma energy by in-vessel coil-current modulation, instead of by isotopic fueling, allows for smaller control actions and finer plasma-energy regulation, provided that a careful controller design is followed. Impurity injection is kept as a backup actuator to decrease the plasma energy provided

that $n \leqslant 2f_{GW}n_{GW}$. By integrating all the feasible actuators within a single algorithm that operates them simultaneously and makes decisions about which one is the most suitable to ensure successful regulation of the burn condition, a more efficient burn controller can be synthesized to overcome the actuation capability limits arising when using individual actuators. To make the proposed nominal nonlinear feedback controller robust against unknown variations in the D–T concentrations of the fueling lines over time such as biases and drifts, the control laws for fueling rate modulation are augmented by following a Lyapunov-redesign approach. Initial work towards this goal has been reported in [18]. In summary, the main contribution of this work is the development of a more complex burn control strategy that is robust against D–T concentration variations in the fueling lines, and that at the same time integrates in-vessel coil-current and controlled impurity injection with the capability of directly controlling the total plasma density. The resulting robust nonlinear feedback controller has been tested in nonlinear simulations for different ITER-like scenarios where its performance is assessed when rejecting initial perturbations, regulating the system around desired operating points, and driving the system between different operating points. Variations in the D–T concentrations of the fueling lines, which are unknown to the controller, have been emulated during the simulations to test the robustness of the control algorithm. Moreover, the performance of the robust nonlinear feedback controller has been compared to the performances of both the nominal nonlinear feedback controller, which is not robust against variations in the D–T concentrations of the fueling lines, and a feedforward control law designed based on the nominal model (not capturing possible variations in the D–T fuel concentrations).

This paper is organized as follows. The nonlinear plasma model is described in section 2, while the control objective is stated in section 3. The controller algorithm is introduced in section 4. The simulation study is presented in section 5. Finally, some conclusions and a discussion on possible future work are given in section 6. Appendices are provided to cover the basics of Lyapunov stability theory (appendix A) and Lyapunov redesign techniques (appendix B).

2. Burning plasma model

The model utilized in this work is a zero-dimensional model in which all variables can be considered as volume-averaged magnitudes. It takes into account the existence of the different types of particles that compose the burning plasma: D, T, α particles, and impurities. Approximate particle density and energy balance equations are employed to characterize the dynamics of the burning plasma. It is assumed in this work that ion and electron temperatures are identical, i.e. $T \triangleq T_e = T_i$, which enables the use of a single energy balance equation in the modeling process. If necessary, this assumption can be relaxed at the expense of a more complex control design.

The balance equations for the D and T densities, n_D and n_T, are given by

$$\frac{dn_D}{dt} = -\frac{n_D}{\tau_D} + f_{eff}S_D^R - S_\alpha + S_D^{inj}, \tag{1}$$

$$\frac{dn_T}{dt} = -\frac{n_T}{\tau_T} + f_{eff}S_T^R - S_\alpha + S_T^{inj}, \tag{2}$$

where t is the time, the terms $-n_D/\tau_D$ and $-n_T/\tau_T$ represent the transport of D and T particles out of the plasma core, respectively, τ_D and τ_T are the D and T confinement times, respectively, S_D^R and S_T^R are the D and T sources from recycling, respectively, f_{eff} is a constant parameter that quantifies the efficiency with which the plasma core is fueled by recycling, S_D^{inj} and S_T^{inj} are the controllable D and T injection rates, respectively, and S_α is the source of α particles arising from nuclear fusion reactions,

$$S_\alpha = n_D n_T \langle\sigma v\rangle = \gamma(1-\gamma)(n_D + n_T)^2\langle\sigma v\rangle, \tag{3}$$

where γ is the tritium fraction, defined as

$$\gamma = n_T/(n_D + n_T), \tag{4}$$

and $\langle\sigma v\rangle$ is the cross section of the D–T reaction, which is modeled as

$$\langle\sigma v\rangle = \exp(a_1/T^r + a_2 + a_3 T + a_4 T^2 + a_5 T^3 + a_6 T^4), \tag{5}$$

where a_i and r are constant scaling parameters [19], and T is the plasma temperature. S_D^R and S_T^R are modeled as in [15],

$$S_D^R = \frac{1}{1 - f_{ref}(1-f_{eff})}\left\{f_{ref}\frac{n_D}{\tau_D} + (1-\gamma_{PFC}) \times \left[\frac{(1-f_{ref}(1-f_{eff}))R_{eff}}{1 - R_{eff}(1-f_{eff})} - f_{ref}\right]\left(\frac{n_D}{\tau_D} + \frac{n_T}{\tau_T}\right)\right\}, \tag{6}$$

$$S_T^R = \frac{1}{1 - f_{ref}(1-f_{eff})}\left\{f_{ref}\frac{n_T}{\tau_T} + (1-\gamma_{PFC}) \times \left[\frac{(1-f_{ref}(1-f_{eff}))R_{eff}}{1 - R_{eff}(1-f_{eff})} - f_{ref}\right]\left(\frac{n_D}{\tau_D} + \frac{n_T}{\tau_T}\right)\right\}, \tag{7}$$

where f_{ref}, R_{eff}, γ_{PFC} are constant parameters that characterize the recycling effects.

The balance equation for the α-particle density, n_α, is given by

$$\frac{dn_\alpha}{dt} = -\frac{n_\alpha}{\tau_\alpha} + S_\alpha, \tag{8}$$

where the term $-n_\alpha/\tau_\alpha$ represents the transport of α particles out of the plasma core, and τ_α is the confinement time of the α particles. For simplicity, only one type of impurity particle is considered in this work, although a more complex model with more types of particles could be used. The time evolution of the impurity particle density, n_I, is given by

$$\frac{dn_I}{dt} = -\frac{n_I}{\tau_I} + S_I^{sp} + S_I^{inj}, \tag{9}$$

where the term $-n_I/\tau_I$ represents the transport of impurities out the plasma core, τ_I is the confinement time of the corresponding impurity particle, S_I^{inj} is the source of impurities

injected for control purposes, and S_I^{sp} is the source of impurities arising from sputtering, which is modeled as

$$S_I^{\mathrm{sp}} = f_I^{\mathrm{sp}}\left(\frac{n}{\tau_I} + \frac{\mathrm{d}n}{\mathrm{d}t}\right), \tag{10}$$

where $f_I^{\mathrm{sp}} > 0$ is a constant parameter, and n is the total plasma density,

$$n = n_i + n_e = 3n_\alpha + 2n_{\mathrm{D}} + 2n_{\mathrm{T}} + (1 + Z_I)n_I, \tag{11}$$

where $n_i = n_\alpha + n_{\mathrm{D}} + n_{\mathrm{T}} + n_I$ is the ion density, and n_e is the electron density, which is related to the density of the ions by the quasi-neutrality condition, $n_e = 2n_\alpha + n_{\mathrm{D}} + n_{\mathrm{T}} + Z_I n_I$, where Z_I is the atomic number of the impurities. The plasma energy, E, is related to n and T by

$$E = \frac{3}{2}(n_i T_i + n_e T_e) = \frac{3}{2}nT, \tag{12}$$

where the assumption $T \triangleq T_e = T_i$ has been used. The energy density balance in the plasma is given by

$$\frac{\mathrm{d}E}{\mathrm{d}t} = -\frac{E}{\tau_{\mathrm{E}}} + P \triangleq -\frac{E}{\tau_{\mathrm{E}}} + P_\alpha + P_{\mathrm{Ohm}} - P_{\mathrm{rad}} + P_{\mathrm{aux}}, \tag{13}$$

where τ_{E} is the energy confinement time, $P \triangleq P_\alpha + P_{\mathrm{Ohm}} - P_{\mathrm{rad}} + P_{\mathrm{aux}}$ is the total power density, P_α is the α-particle heating power density, P_{Ohm} is the ohmic heating power density, P_{rad} is the radiative power density, and P_{aux} is the auxiliary power density injected into the plasma. The α-particle power is given by $P_\alpha = Q_\alpha S_\alpha$, where $Q_\alpha = 3.52$ MeV. The ohmic power is given by $P_{\mathrm{Ohm}} = 2.8 \times 10^{-9}(Z_{\mathrm{eff}} I_{\mathrm{p}}^2)/(a^4 T^{3/2})$, where $Z_{\mathrm{eff}} = (4n_\alpha + n_{\mathrm{D}} + n_{\mathrm{T}} + Z_I^2 n_I)/n_e$ is the effective atomic number of the plasma ions, I_{p} is the plasma current, a is the minor radius of the tokamak, and T has to be given in keV. The radiative power is composed by three terms, $P_{\mathrm{rad}} = P_{\mathrm{brem}} + P_{\mathrm{line}} + P_{\mathrm{rec}}$, where P_{brem} is the Bremsstrahlung term, P_{line} is the line radiation term, and P_{rec} is the recombination term. Each term is given by $P_{\mathrm{brem}} = 4.8 \times 10^{-37}\left(\sum_j n_j Z_j^2\right) n_e \sqrt{T}$, $P_{\mathrm{line}} = 1.8 \times 10^{-38}\left(\sum_j n_j Z_j^4\right) n_e T^{-1/2}$, and $P_{\mathrm{rec}} = 4.1 \times 10^{-40}\left(\sum_j n_j Z_j^6\right) n_e T^{-3/2}$, where the summation in j is done for all types of ions in the plasma, and T has to be given in keV [20].

2.1. Effect of in-vessel coil currents on energy confinement time

For τ_{E}, the IPB98(y,2) scaling is used [21],

$$\tau_{\mathrm{E}} = 0.0562 H_{\mathrm{H}} I_{\mathrm{p}}^{0.93} B_{\mathrm{T}}^{0.15} n_{\mathrm{e19}}^{0.41} M^{0.19} \times R^{1.39} a^{0.58} \kappa_{95}^{0.78} (PV)^{-0.69}, \tag{14}$$

where H_{H} is the so-called H-factor, I_{p} is the plasma current in MA, B_{T} is the toroidal magnetic field, $n_{e,19}$ is the electron density in 10^{19} m^{-3}, $M = (2n_{\mathrm{D}} + 3n_{\mathrm{T}})/(n_{\mathrm{D}} + n_{\mathrm{T}})$ is the plasma effective mass in amu, R is the major radius, a is the minor radius, κ_{95} is the elongation at the 95% flux surface/separatrix, P is the total power density in MW m^{-3}, and V is the plasma volume. It is assumed that all particle confinement times scale with τ_{E}, i.e. $\tau_\alpha = k_\alpha \tau_{\mathrm{E}}$, $\tau_{\mathrm{D}} = k_{\mathrm{D}} \tau_{\mathrm{E}}$, $\tau_{\mathrm{T}} = k_{\mathrm{T}} \tau_{\mathrm{E}}$, $\tau_I = k_I \tau_{\mathrm{E}}$, where k_α, k_{D}, k_{T} and k_I are constant parameters.

The H-factor, H_{H}, is a scalar which represents the uncertainty of the IPB98(y,2) scaling under different scenarios and operating conditions. A value of $H_{\mathrm{H}} = 1$ yields the best fit to experimental data in the international database. It can also be seen as a measurement of the plasma confinement quality which comprises effects not explicitly included in the IPB98(y,2) scaling. Amongst those effects, perturbations in the tokamak magnetic configuration can be considered. In particular, those magnetic perturbations introduced by the non-axisymmetric magnetic fields generated by the in-vessel coils have a proven impact on H_{H} in DIII-D plasmas with relatively low normalized collisionality ν_e and relatively low n_e ($\nu_e \approx 0.1$, $n_e \approx 3.5 \times 10^{19}$ m^{-3}) [7]. In these experiments, activation of the in-vessel coils implied a decrease in H_{H} and, consequently, a decrease in τ_{E}. Tokamak plasmas with higher ν_e and n_e, on the contrary, did not show H_{H} variations under application of non-axisymmetric magnetic fields [8]. Using the experimental data available for DIII-D in [7, 8], the influence on H_{H} of the in-vessel-coil current, denoted as I_{coil} (assuming that all in-vessel coils are configured to have the same current), is modeled by using a control-oriented scaling given by

$$H_{\mathrm{H}} = H_{\mathrm{H},0} + \left(\frac{n_e}{n_{e,0}}\right)^{-\delta}\left(\frac{\nu_e}{\nu_{e,0}}\right)^{-\lambda} \times \left[C_2 I_{\mathrm{coil}}^2 + C_1 I_{\mathrm{coil}}\right], \tag{15}$$

where $H_{\mathrm{H},0}$ is the H-factor without activation of the in-vessel coils, $n_{e,0}$ and $\nu_{e,0}$ are the electron density and collisionality, respectively, corresponding to a nominal working point for which experimental data is available, and $\delta > 0$, $\lambda > 0$, C_1 and C_2 are constants which are determined from the experimental data. Because the in-vessel coils can only reduce H_{H}, the term $\left[C_2 I_{\mathrm{coil}}^2 + C_1 I_{\mathrm{coil}}\right]$ is always $\leqslant 0$, $\forall I_{\mathrm{coil}} \geqslant 0$.

2.2. Uncertainty characterization for the D–T concentration in the fueling lines

The fueling rates associated with the two fueling lines available in the initial phase of ITER (D–T pellet injector and D pellet injector) are denoted as $S_{\mathrm{DT\text{-}line}}^{\mathrm{inj}}$ and $S_{\mathrm{D\text{-}line}}^{\mathrm{inj}}$, respectively, and are considered as directly controllable magnitudes. $S_{\mathrm{D}}^{\mathrm{inj}}$ and $S_{\mathrm{T}}^{\mathrm{inj}}$ can be expressed, in terms of $S_{\mathrm{DT\text{-}line}}^{\mathrm{inj}}$ and $S_{\mathrm{D\text{-}line}}^{\mathrm{inj}}$, as

$$S_{\mathrm{D}}^{\mathrm{inj}} = (1 - \gamma_{\mathrm{D\text{-}line}}) S_{\mathrm{D\text{-}line}}^{\mathrm{inj}} + (1 - \gamma_{\mathrm{DT\text{-}line}}) S_{\mathrm{DT\text{-}line}}^{\mathrm{inj}}, \tag{16}$$

$$S_{\mathrm{T}}^{\mathrm{inj}} = \gamma_{\mathrm{D\text{-}line}} S_{\mathrm{D\text{-}line}}^{\mathrm{inj}} + \gamma_{\mathrm{DT\text{-}line}} S_{\mathrm{DT\text{-}line}}^{\mathrm{inj}}, \tag{17}$$

where $\gamma_{\mathrm{DT\text{-}line}} \in [0, 1]$ and $\gamma_{\mathrm{D\text{-}line}} \in [0, 1]$ are parameters that characterize the T concentration in the D–T and D pellet injectors, respectively. Therefore, in the nominal case, $\gamma_{\mathrm{DT\text{-}line}} = \gamma_{\mathrm{DT\text{-}line}}^{\mathrm{nom}} \triangleq 0.9$ and $\gamma_{\mathrm{D\text{-}line}} = \gamma_{\mathrm{D\text{-}line}}^{\mathrm{nom}} \triangleq 0$. However, as introduced above, unknown variations over time in the D–T concentrations are expected in the fueling lines. Such uncertainties are modeled as

$$\gamma_{\mathrm{D\text{-}line}} = \gamma_{\mathrm{D\text{-}line}}^{\mathrm{nom}} + \delta_{\mathrm{D\text{-}line}}, \tag{18}$$

$$\gamma_{\mathrm{DT\text{-}line}} = \gamma_{\mathrm{DT\text{-}line}}^{\mathrm{nom}} + \delta_{\mathrm{DT\text{-}line}}, \tag{19}$$

Table 1. ITER parameters [21].

Symbol	Description	Value
I_p	Plasma current	15.0 MA
R	Major radius	6.2 m
a	Minor radius	2.0 m
B_T	Magnetic field	5.3 T
κ_{95}	Elongation at 95% flux surface/separatrix	1.7
V	Plasma volume	837 m^3
ν_e	Normalized electron collisionality	0.1

where $\delta_{\text{DT-line}}$ and $\delta_{\text{D-line}}$ are the unknown variations in the D–T concentration in the D–T and D pellet injectors, respectively. From its definition, it is found that $\delta_{\text{DT-line}} \in [-0.9, 0.1]$ and $\delta_{\text{D-line}} \in [0, 1]$, so these uncertainties are bounded.

2.3. Total density and tritium fraction dynamics

By using (16) and (17), equations (1) and (2) can be rewritten in terms of the inputs to the system $S^{\text{inj}}_{\text{D-line}}$ and $S^{\text{inj}}_{\text{DT-line}}$ as

$$\frac{dn_D}{dt} = -\frac{n_D}{\tau_D} + f_{\text{eff}} S^R_D - S_\alpha + (1-\gamma_{\text{D-line}}) S^{\text{inj}}_{\text{D-line}} + (1-\gamma_{\text{DT-line}}) S^{\text{inj}}_{\text{DT-line}}, \tag{20}$$

$$\frac{dn_T}{dt} = -\frac{n_T}{\tau_T} + f_{\text{eff}} S^R_T - S_\alpha + \gamma_{\text{D-line}} S^{\text{inj}}_{\text{D-line}} + \gamma_{\text{DT-line}} S^{\text{inj}}_{\text{DT-line}}. \tag{21}$$

Because isotopic fueling controls E by regulating γ, and stability limits exist for n, it may be convenient to control n and γ instead of n_D and n_T when using this fueling technique. From (4), (11), and the balance equations (8), (9), (20), (21), it is possible to write the balance equations for n and γ, which are given by

$$\frac{dn}{dt} = 3\left(-\frac{n_\alpha}{\tau_\alpha} + S_\alpha\right) + [3n_\alpha + (1+Z_I)\, n_I - n] \left(\frac{1-\gamma}{\tau_D} + \frac{\gamma}{\tau_T}\right) + 2f_{\text{eff}}\left(S^R_D + S^R_T\right) - 4S_\alpha + 2(S^{\text{inj}}_{\text{D-line}} + S^{\text{inj}}_{\text{DT-line}}) + (1+Z_I)\left(-\frac{n_I}{\tau_I} + S^{\text{inj}}_I + S^{\text{sp}}_I\right), \tag{22}$$

$$\frac{d\gamma}{dt} = \gamma(1-\gamma)\left(\frac{1}{\tau_D} - \frac{1}{\tau_T}\right) + \frac{2}{n - 3n_\alpha - (1+Z_I)\, n_I} \left[f_{\text{eff}} S^R_T - S_\alpha + \gamma_{\text{D-line}} S^{\text{inj}}_{\text{D-line}} + \gamma_{\text{DT-line}} S^{\text{inj}}_{\text{DT-line}} - \gamma \left(f_{\text{eff}}\left(S^R_D + S^R_T\right) - 2S_\alpha + S^{\text{inj}}_{\text{D-line}} + S^{\text{inj}}_{\text{DT-line}}\right)\right]. \tag{23}$$

A a result, two states, x, are utilized in this work for control design.

(i) If fueling rate modulation directly controls n_D and n_T, then $x = [n_\alpha, n_D, n_T, n_I, E]^T$.
(ii) If isotopic fuel tailoring controls n and γ, then $x = [n_\alpha, n, \gamma, n_I, E]^T$.

Table 2. Model variables.

Symbol	Description	Type of variable
n_α, n_D, n_T, n_I	Particle densities	State
E	Plasma energy density	State
γ	Tritium fraction	Intermediate variable
n_e, n_i, n	Electron, ion, and total density	Intermediate variable
Z_{eff}	Effective atomic number	Intermediate variable
M	Plasma effective mass	Intermediate variable
T	Plasma temperature	Intermediate variable
β_t, β_N	Toroidal and normalized plasma beta	Intermediate variable
S_α	Source of α particles from fusion	Intermediate variable
$\langle\sigma v\rangle$	Reactivity	Intermediate variable
S^R_D, S^R_T	Recycling D and T sources	Intermediate variable
S^{inj}_D, S^{inj}_T	Injected D and T sources	Intermediate variable
S^{sp}_I	Sputtering source	Intermediate variable
P_α, P_{Ohm}, P_{rad}	α, Ohmic, and radiative heating sources	Intermediate variable
τ_E, τ_α, τ_D, τ_T, τ_I	Confinement times	Intermediate variable
$S^{\text{inj}}_{\text{D-line}}$, $S^{\text{inj}}_{\text{DT-line}}$	D and DT pellet injection rates	Controllable input
S^{inj}_I	Impurity injection rate	Controllable input
I_{coil}	In-vessel coil current	Controllable input
P_{aux}	Auxiliary heating	Controllable input
I_p, R, a, B_T, κ_{95}, V, ν_e	Machine parameters	Machine parameter
a_i, r	Reactivity constants	Model parameter
Z_I	Impurity atomic number	Model parameter
k_α, k_D, k_T, k_I	Confinement time constants	Model parameter
f_{eff}, R_{eff}, f_{ref}, γ_{PFC}, f^{sp}_I	Recycling & sputtering constants	Model parameter
$H_{\text{H},0}$, C_i, λ, δ, $n_{e,0}$, $\nu_{e,0}$	In-vessel coil-model constants	Model parameter
$\gamma^{\text{nom}}_{\text{D-line}}$, $\gamma^{\text{nom}}_{\text{DT-line}}$	Nominal pellet concentrations	Model parameter
$\delta_{\text{D-line}}$, $\delta_{\text{DT-line}}$	Uncertain pellet concentrations	Uncertain variables

The inputs to the system are P_{aux}, I_{coil}, S^{inj}_I, $S^{\text{inj}}_{\text{D-line}}$, and $S^{\text{inj}}_{\text{DT-line}}$. To close the model, it is necessary to specify the machine parameters. ITER is the machine considered in this work, and its parameters are given in table 1. Moreover, the variables employed in this nonlinear model of the burning plasma are summarized in table 2. Also, a diagram illustrating

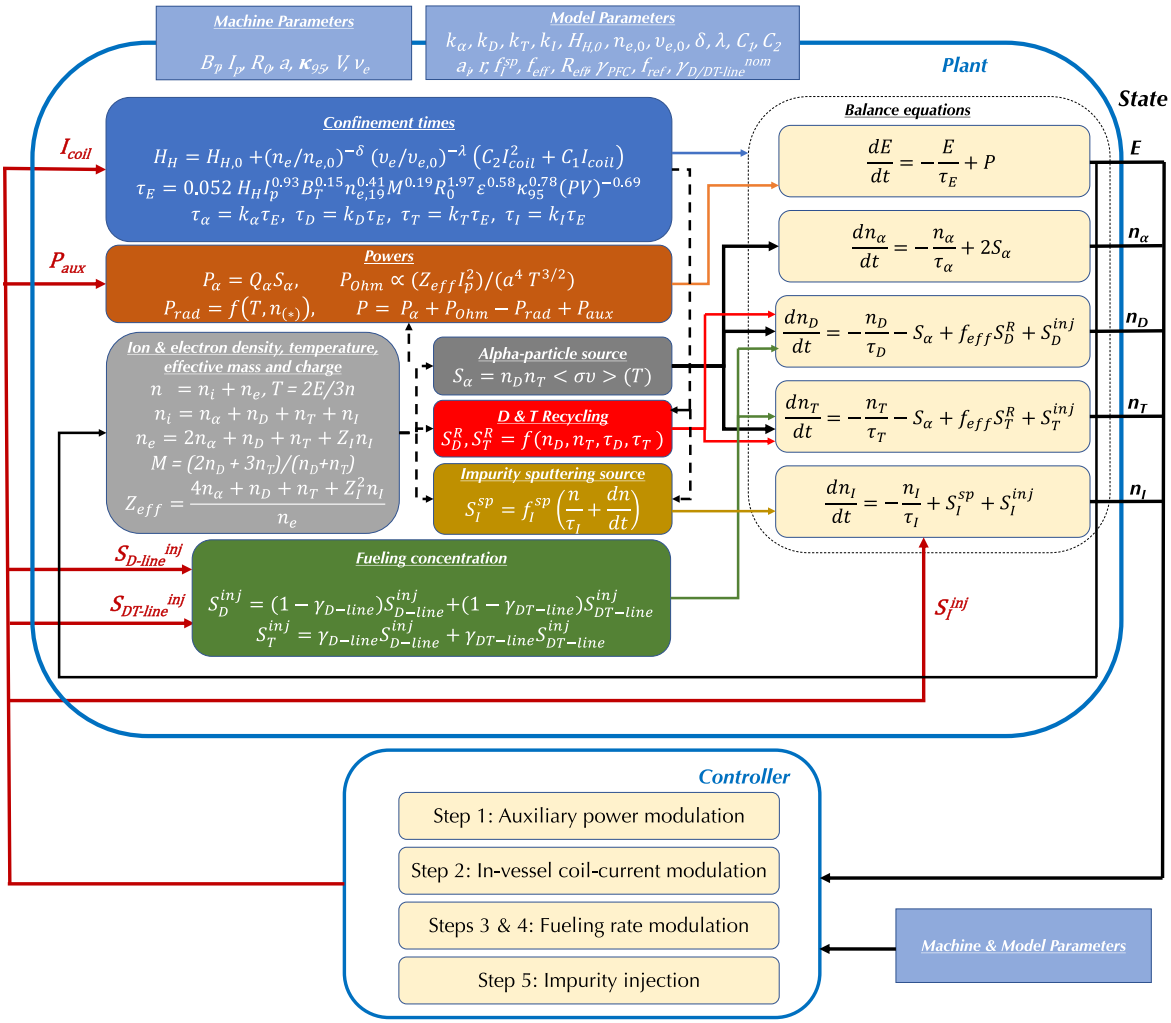

Figure 1. Diagram for the burning-plasma plant and its connection with the controller.

the relationship between these variables, as well as their connection with the nonlinear burn controller presented in section 4, is shown in figure 1.

3. Operating points and control objective

The equilibria of the balance equations (8), (9), (13), (20), (21) (or alternatively, (8), (9), (13), (22) and (23)), which define the operating points of the tokamak, are obtained by setting the time derivatives to zero. Upper bars are used to denote equilibrium values. As no controlled impurity injection is desired at equilibrium, $\bar{S}_I^{\mathrm{inj}} \equiv 0$ is set. In addition, at any operating point, it is desirable that $\bar{\tau}_{\mathrm{E}}$ is as large as possible, thus $\bar{I}_{\mathrm{coil}} \equiv 0$ is imposed. Then, the equilibrium system is composed by five equations with eight unknowns (five state variables + three inputs), so three variables must be specified in order to find a unique solution.

The variables fixed in this work to solve for the equilibrium, and therefore define the tokamak operating points, are $T = \bar{T}$, $\gamma = \bar{\gamma}$, and $\beta_N = \bar{\beta}_N$, where

$$\beta_N = \beta_t \frac{aB_{\mathrm{T}}}{I_{\mathrm{p}}}[\%],\ \beta_t = \frac{\frac{4}{3}\mu_0 E}{B_{\mathrm{T}}^2}, \tag{24}$$

where μ_0 is the vacuum permeability. The dynamic equations for the state error, defined as $\tilde{x} \triangleq x - \bar{x}$, are given by

$$\frac{\mathrm{d}\tilde{n}_\alpha}{\mathrm{d}t} = -\frac{\bar{n}_\alpha}{\tau_\alpha} - \frac{\tilde{n}_\alpha}{\tau_\alpha} + S_\alpha, \tag{25}$$

$$\frac{\mathrm{d}\tilde{n}_{\mathrm{D}}}{\mathrm{d}t} = -\frac{\bar{n}_{\mathrm{D}}}{\tau_{\mathrm{D}}} - \frac{\tilde{n}_{\mathrm{D}}}{\tau_{\mathrm{D}}} + f_{\mathrm{eff}} S_{\mathrm{D}}^R - S_\alpha + (1-\gamma_{\mathrm{D\text{-}line}}) \times S_{\mathrm{D\text{-}line}}^{\mathrm{inj}} + (1-\gamma_{\mathrm{DT\text{-}line}}) S_{\mathrm{DT\text{-}line}}^{\mathrm{inj}}, \tag{26}$$

$$\frac{\mathrm{d}\tilde{n}_{\mathrm{T}}}{\mathrm{d}t} = -\frac{\bar{n}_{\mathrm{T}}}{\tau_{\mathrm{T}}} - \frac{\tilde{n}_{\mathrm{T}}}{\tau_{\mathrm{T}}} + f_{\mathrm{eff}} S_{\mathrm{T}}^R - S_\alpha + \gamma_{\mathrm{D\text{-}line}} S_{\mathrm{D\text{-}line}}^{\mathrm{inj}} + \gamma_{\mathrm{DT\text{-}line}} S_{\mathrm{DT\text{-}line}}^{\mathrm{inj}}, \tag{27}$$

$$\frac{\mathrm{d}\tilde{n}_I}{\mathrm{d}t} = -\frac{\bar{n}_I}{\tau_I} - \frac{\tilde{n}_I}{\tau_I} + S_I^{\mathrm{inj}} + S_I^{\mathrm{sp}}, \tag{28}$$

$$\frac{\mathrm{d}\tilde{E}}{\mathrm{d}t} = -\frac{\bar{E}}{\tau_E} - \frac{\tilde{E}}{\tau_E} + P_\alpha + P_{\mathrm{Ohm}} - P_{\mathrm{rad}} + P_{\mathrm{aux}}, \tag{29}$$

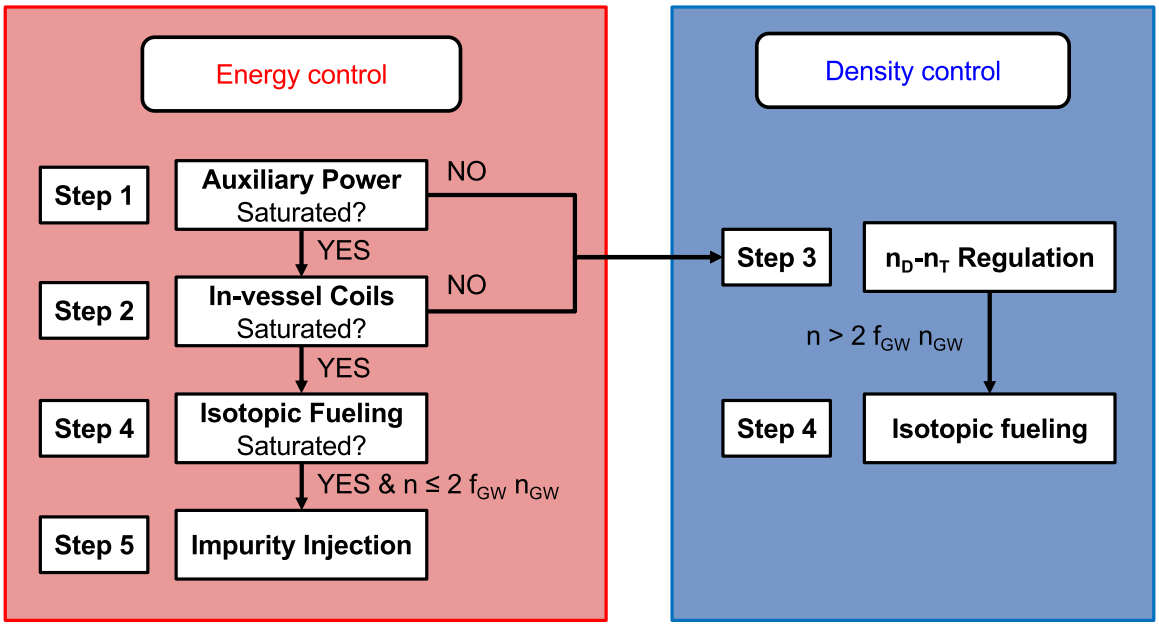

Figure 2. Utilization of the different actuation methods within the burn controller. Each actuation method is associated with a particular step of the control algorithm.

if $\tilde{x} = [\tilde{n}_\alpha, \tilde{n}_\mathrm{D}, \tilde{n}_\mathrm{T}, \tilde{n}_I, \tilde{E}]^T$ (isotopic fueling is not used). If $\tilde{x} = [\tilde{n}_\alpha, \tilde{n}, \tilde{\gamma}, \tilde{n}_I, \tilde{E}]^T$ (isotopic fueling is used), then (26) and (27) are substituted by

$$\begin{aligned}\frac{\mathrm{d}\tilde{n}}{\mathrm{d}t} &= 3\left(-\frac{\tilde{n}_\alpha}{\tau_\alpha} - \frac{\bar{n}_\alpha}{\tau_\alpha} + S_\alpha\right) + 2f_\mathrm{eff}\left(S^R_\mathrm{D} + S^R_\mathrm{T}\right) - 4S_\alpha \\ &+ \left[3\left(\bar{n}_\alpha + \tilde{n}_\alpha\right) + (1+Z_I)\left(\bar{n}_I + \tilde{n}_I\right) - \left(\bar{n} + \tilde{n}\right)\right]\left(\frac{1-(\bar{\gamma}+\tilde{\gamma})}{\tau_\mathrm{D}} + \frac{(\bar{\gamma}+\tilde{\gamma})}{\tau_\mathrm{T}}\right) \\ &+ 2\left(S^\mathrm{inj}_\text{D-line} + S^\mathrm{inj}_\text{DT-line}\right) + (1+Z_I)\left(-\frac{\bar{n}_I}{\tau_I} - \frac{\tilde{n}_I}{\tau_I} + S^\mathrm{inj}_I + S^\mathrm{sp}_I\right), \quad (30)\end{aligned}$$

$$\begin{aligned}\frac{\mathrm{d}\tilde{\gamma}}{\mathrm{d}t} &= (\bar{\gamma}+\tilde{\gamma})(1-(\bar{\gamma}+\tilde{\gamma}))\left(\frac{1}{\tau_\mathrm{D}} - \frac{1}{\tau_\mathrm{T}}\right) \\ &+ \frac{2}{\bar{n}+\tilde{n} - 3(\bar{n}_\alpha+\tilde{n}_\alpha) - (1+Z_I)\left(\bar{n}_I+\tilde{n}_I\right)} \\ &\times\left\{f_\mathrm{eff}S^R_\mathrm{T} - S_\alpha + \gamma_\text{D-line}S^\mathrm{inj}_\text{D-line} + \gamma_\text{DT-line}S^\mathrm{inj}_\text{DT-line}\right. \\ &\left. - (\bar{\gamma}+\tilde{\gamma})\left[f_\mathrm{eff}\left(S^R_\mathrm{D} + S^R_\mathrm{T}\right) - 2S_\alpha + S^\mathrm{inj}_\text{D-line} + S^\mathrm{inj}_\text{DT-line}\right]\right\}. \quad (31)\end{aligned}$$

The control objective is to drive the state error $\tilde{x}$ to zero, i.e. to drive the state x to its equilibrium value $\bar{x}$.

4. Controller design

4.1. Nominal control law ($\delta_\text{D-line} = 0$, $\delta_\text{DT-line} = 0$)

A controller for the nominal system ($\delta_\text{D-line} = 0$, $\delta_\text{DT-line} = 0$) is designed in this section by using Lyapunov techniques (see appendix A). As shown in figure 1, it is assumed that the states are available for feedback control (either measured by plasma diagnostics or estimated by a state observer). Each actuation method is employed in accordance with the flowchart showed in figure 2. First, the nominal controller attempts to regulate $\tilde{E}$ by using auxiliary power modulation. If P_aux saturates, then in-vessel coil-current modulation is used. If in-vessel coil-current modulation saturates as well, then fueling rate modulation is used to attempt to control $\tilde{E}$ and $\tilde{n}$ by isotopic fueling. On the other hand, if auxiliary power modulation and/or in-vessel coil-current modulation suffice to regulate $\tilde{E}$ without saturation, then fueling rate modulation is used to control $\tilde{n}_\mathrm{D}$ and $\tilde{n}_\mathrm{T}$, except if too high values of n are found. In order to prevent n from reaching excessively high values that may trigger instabilities, isotopic fueling is used when the Greenwald density limit, denoted as n_GW, is close to be reached. Finally, in case isotopic fueling is used but $\tilde{E}$ and $\tilde{n}$ regulation cannot be ensured, impurity injection is employed to regulate $\tilde{E}$. Stability proofs are provided to show that if $\tilde{E}$, $\tilde{n}_\mathrm{D}$, and $\tilde{n}_\mathrm{T}$ (or, alternatively, $\tilde{E}$, γ, and $\tilde{n}$ when isotopic fueling is used) are successfully regulated, then $\tilde{n}_\alpha$ and $\tilde{n}_I$ converge to zero as well.

Step 1: Auxiliary power modulation. If P_aux is set to

$$P^\mathrm{unsat}_\mathrm{aux} = \frac{\bar{E}}{\tau_E} - P_\alpha - P_\mathrm{Ohm} + P_\mathrm{rad} - K_P\tilde{E}, \quad (32)$$

where $K_P > 0$ is a design parameter, then (29) is reduced to $\mathrm{d}\tilde{E}/\mathrm{d}t = -\left(1/\tau_\mathrm{E} + K_P\right)\tilde{E}$, and using a Lyapunov function [22] $V_{\tilde{E}} = \frac{1}{2}\tilde{E}^2 > 0$, yields $\dot{V}_{\tilde{E}} = -\left(1/\tau_\mathrm{E} + K_P\right)\tilde{E}^2 < 0$. This ensures global asymptotical stability for $\tilde{E}$ (i.e. $\tilde{E} \to 0$). Equation (32) represents the control law for P_aux. When $P_\mathrm{aux} = P^\mathrm{unsat}_\mathrm{aux}$, neither in-vessel coil-current modulation (Step 2) nor impurity injection (Step 5) are used, i.e. $I_\mathrm{coil} \equiv 0$ and $S^\mathrm{inj}_I \equiv 0$. Moreover, $\tilde{n}_\mathrm{D}$ and $\tilde{n}_\mathrm{T}$ are controlled by fueling rate modulation (Step 3) as long as $n \leqslant 2f_\mathrm{GW}n_\mathrm{GW}$, where $n_\mathrm{GW} = \frac{I_\mathrm{p}}{\pi a^2}10^{20}$ m^{-3} is the Greenwald density limit (I_p in MA), and $0 < f_\mathrm{GW} \leqslant 1$ is a design parameter. Otherwise, $\tilde{n}_\mathrm{D}$ and $\tilde{n}_\mathrm{T}$ are controlled by isotopic fueling (Step 4). However, it may not be possible

to set $P_{\text{aux}} = P_{\text{aux}}^{\text{unsat}}$ as requested by (32) because there exist saturation limits, which are denoted as $P_{\text{aux}}^{\max}$ and $P_{\text{aux}}^{\min}$. If $P_{\text{aux}}^{\text{unsat}} > P_{\text{aux}}^{\max}$, the control algorithm keeps $P_{\text{aux}} = P_{\text{aux}}^{\max}$, but it cannot be ensured that $\tilde{E} \to 0$. The only possible ways to cope with this limitation are either increasing $P_{\text{aux}}^{\max}$ or improving the machine parameters (I_{p}, B_{T}, R, a, κ_{95}, etc) to enhance confinement. On the other hand, if $P_{\text{aux}}^{\text{unsat}} < P_{\text{aux}}^{\min}$, the control algorithm keeps $P_{\text{aux}} = P_{\text{aux}}^{\min}$, but it cannot be ensured that $\tilde{E} \to 0$. In that case, the controller is designed to use in-vessel coil-current modulation (Step 2), isotopic fueling (Step 4), and/or impurity injection (Step 5) to regulate $\tilde{E}$, in this order.

Step 2: In-vessel coil-current modulation. If τ_{E} is set to

$$\tau_{\text{E}}^{\text{unsat}} = \frac{\bar{E}}{P^{\min} + K_{\tau_{\text{E}}}\tilde{E}}, \tag{33}$$

where $P^{\min} = P_{\alpha} + P_{\text{Ohm}} - P_{\text{rad}} + P_{\text{aux}}^{\min}$, and $K_{\tau_{\text{E}}} > 0$ is a design parameter, then (29) is reduced to $\mathrm{d}\tilde{E}/\mathrm{d}t = -\left(1/\tau_{\text{E}} + K_{\tau_{\text{E}}}\right)\tilde{E}$. Using $V_{\tilde{E}} = \frac{1}{2}\tilde{E}^2 > 0$, then $\dot{V}_{\tilde{E}} = -\left(1/\tau_{\text{E}} + K_{\tau_{\text{E}}}\right)\tilde{E}^2 < 0$, which ensures global asymptotical stability for $\tilde{E}$ (i.e. $\tilde{E} \to 0$). The required value $I_{\text{coil}}^{\text{unsat}}$ to set τ_{E} as in (33) is obtained from (14), (15) and (33) by solving the following nonlinear equation,

$$C_2(I_{\text{coil}}^{\text{unsat}})^2 + C_1 I_{\text{coil}}^{\text{unsat}} = \left(\frac{\tau_{\text{E}}^{\text{unsat}}}{K_{\text{IPB98(y,2)}}} - H_{\text{H,0}}\right)\left(\frac{n_e}{n_{e,0}}\right)^{\delta}\left(\frac{\nu_e}{\nu_{e,0}}\right)^{\lambda}, \tag{34}$$

where $K_{\text{IPB98(y,2)}} = 0.0562 I_{\text{p}}^{0.93} B_{\text{T}}^{0.15} n_{e,19}^{0.41} M^{0.19} R^{1.39} a^{0.58} \kappa_{95}^{0.78} (P^{\min})^{-0.69} V^{-0.69}$. As in Step 1, the right hand side of (34) can be computed, providing the control law for I_{coil}. When $I_{\text{coil}} = I_{\text{coil}}^{\text{unsat}}$, $\tilde{n}_{\text{D}}$ and $\tilde{n}_{\text{T}}$ are controlled by fueling rate modulation (Step 3), except if $n > 2 f_{\text{GW}} n_{\text{GW}}$, when again isotopic fueling (Step 4) is activated. However, it may not be possible to set $I_{\text{coil}} = I_{\text{coil}}^{\text{unsat}}$ because there exist saturation limits, i.e. $0 \leqslant I_{\text{coil}} \leqslant I_{\text{coil}}^{\max}$. $I_{\text{coil}}^{\text{unsat}} \leqslant 0$ is an indication that indeed there is no need to decrease τ_{E}. In this case, in-vessel coil-current modulation is not necessary and the controller makes $I_{\text{coil}} \equiv 0$. On the other hand, if $I_{\text{coil}}^{\text{unsat}} > I_{\text{coil}}^{\max}$, the controller sets $I_{\text{coil}} = I_{\text{coil}}^{\max}$ and uses isotopic fueling (Step 4) and impurity injection (Step 5) to further regulate $\tilde{E}$, as needed.

Step 3: Fueling rate modulation ($\tilde{n}_{\text{D}}$ and $\tilde{n}_{\text{T}}$ control). If $S_{\text{D}}^{\text{inj}}$ and $S_{\text{T}}^{\text{inj}}$ are set to

$$S_{\text{D}}^{\text{inj,unsat}} = -f_{\text{eff}} S_{\text{D}}^{R} + S_{\alpha} + \frac{\bar{n}_{\text{D}}}{\tau_{\text{D}}} - K_{\text{D}}\tilde{n}_{\text{D}}, \tag{35}$$

$$S_{\text{T}}^{\text{inj,unsat}} = -f_{\text{eff}} S_{\text{T}}^{R} + S_{\alpha} + \frac{\bar{n}_{\text{T}}}{\tau_{\text{T}}} - K_{\text{T}}\tilde{n}_{\text{T}}, \tag{36}$$

where $K_{\text{D}} > 0$ and $K_{\text{T}} > 0$ are design parameters, then (26) and (27) are reduced to $\mathrm{d}\tilde{n}_{\text{D}}/\mathrm{d}t = -\left(1/\tau_{\text{D}} + K_{\text{D}}\right)\tilde{n}_{\text{D}}$ and $\mathrm{d}\tilde{n}_{\text{T}}/\mathrm{d}t = -\left(1/\tau_{\text{T}} + K_{\text{T}}\right)\tilde{n}_{\text{T}}$, respectively. Using $V_{\tilde{n}_{\text{D}}} = \frac{1}{2}\tilde{n}_{\text{D}}^2$ and $V_{\tilde{n}_{\text{T}}} = \frac{1}{2}\tilde{n}_{\text{T}}^2$, it is found that $\dot{V}_{\tilde{n}_{\text{D}}} = -\left(1/\tau_{\text{D}} + K_{\text{D}}\right)\tilde{n}_{\text{D}}^2$ and $\dot{V}_{\tilde{n}_{\text{T}}} = -\left(1/\tau_{\text{T}} + K_{\text{T}}\right)\tilde{n}_{\text{T}}^2 < 0$, thus both $\tilde{n}_{\text{D}}$ and $\tilde{n}_{\text{T}}$ evolutions are globally asymptotically stable (i.e. $\tilde{n}_{\text{D}} \to 0$ and $\tilde{n}_{\text{T}} \to 0$). The stabilizing values for $S_{\text{D-line}}^{\text{inj}}$ and $S_{\text{DT-line}}^{\text{inj}}$ are obtained by solving (16), (17) together with (35), (36), and are given by

$$S_{\text{D-line}}^{\text{inj,unsat}} = \frac{1}{\gamma_{\text{DT-line}}^{\text{nom}} - \gamma_{\text{D-line}}^{\text{nom}}}\left(\gamma_{\text{DT-line}}^{\text{nom}}\left(-f_{\text{eff}} S_{\text{D}}^{R} + S_{\alpha} + \frac{\bar{n}_{\text{D}}}{\tau_{\text{D}}} - K_{\text{D}}\tilde{n}_{\text{D}}\right) - \gamma_{\text{D-line}}^{\text{nom}}\left(-f_{\text{eff}} S_{\text{T}}^{R} + S_{\alpha} + \frac{\bar{n}_{\text{T}}}{\tau_{\text{T}}} - K_{\text{T}}\tilde{n}_{\text{T}}\right)\right), \tag{37}$$

$$S_{\text{DT-line}}^{\text{inj,unsat}} = \frac{1}{\gamma_{\text{DT-line}}^{\text{nom}} - \gamma_{\text{D-line}}^{\text{nom}}}\left(\gamma_{\text{DT-line}}^{\text{nom}}\left(-f_{\text{eff}} S_{\text{D}}^{R} + S_{\alpha} + \frac{\bar{n}_{\text{D}}}{\tau_{\text{D}}} - K_{\text{D}}\tilde{n}_{\text{D}}\right) - \gamma_{\text{D-line}}^{\text{nom}}\left(-f_{\text{eff}} S_{\text{T}}^{R} + S_{\alpha} + \frac{\bar{n}_{\text{T}}}{\tau_{\text{T}}} - K_{\text{T}}\tilde{n}_{\text{T}}\right) + f_{\text{eff}}\left(S_{\text{D}}^{R} - S_{\text{T}}^{R}\right) + \frac{\bar{n}_{\text{T}}}{\tau_{\text{T}}} - \frac{\bar{n}_{\text{D}}}{\tau_{\text{D}}} + K_{\text{D}}\tilde{n}_{\text{D}} - K_{\text{T}}\tilde{n}_{\text{T}}\right). \tag{38}$$

Equations (37) and (38) are the nominal control laws for $S_{\text{DT-line}}^{\text{inj}}$ and $S_{\text{D-line}}^{\text{inj}}$, respectively, when Step 3 is activated. Nonetheless, as before, it may not be possible to set $S_{\text{D-line}}^{\text{inj}} = S_{\text{D-line}}^{\text{inj,unsat}}$ and/or $S_{\text{DT-line}}^{\text{inj}} = S_{\text{DT-line}}^{\text{inj,unsat}}$ because there exist physical saturation limits, that are denoted by $S_{\text{D-line}}^{\text{inj,max}}$, $S_{\text{D-line}}^{\text{inj,min}}$, $S_{\text{DT-line}}^{\text{inj,max}}$, and $S_{\text{DT-line}}^{\text{inj,min}}$. If $S_{\text{D-line}}^{\text{inj}}/S_{\text{DT-line}}^{\text{inj}}$ is larger or smaller than its applicable saturation limits, the controller keeps $S_{\text{D-line}}^{\text{inj}}/S_{\text{DT-line}}^{\text{inj}}$ at the saturation limit that has been violated, and no further steps in the control algorithm are activated. The asymptotic stability of $\tilde{n}_{\text{D}}$ and/or $\tilde{n}_{\text{T}}$ cannot be ensured unless the controller recovers from the saturation limits. This is not an inherent problem of the control algorithm but just a physical limitation in the actuation capability of the tokamak.

Finally, it can be shown that, if $\tilde{E}$, $\tilde{n}_{\text{D}}$, and $\tilde{n}_{\text{T}}$ are driven to zero, i.e. if $E = \bar{E}$, $n_{\text{D}} = \bar{n}_{\text{D}}$, and $n_{\text{T}} = \bar{n}_{\text{T}}$, then $\tilde{n}_{\alpha}$ and $\tilde{n}_I$ are also driven to zero as $t \to \infty$ provided that $S_I^{\text{inj}} \equiv 0$. First, by defining $\hat{n}_I \triangleq n_I - f_I^{\text{sp}} n$, (9) can be rewritten as

$$\frac{\mathrm{d}\hat{n}_I}{\mathrm{d}t} + f_I^{\text{sp}}\frac{\mathrm{d}n}{\mathrm{d}t} = -\frac{\hat{n}_I + f_I^{\text{sp}} n}{\tau_I} + S_I^{\text{sp}}, \tag{39}$$

and using (10), it is found that

$$\frac{\mathrm{d}\hat{n}_I}{\mathrm{d}t} = -\frac{\hat{n}_I}{\tau_I}. \tag{40}$$

Thus, $\hat{n}_I$ goes to zero as $t \to \infty$ because $\tau_I > 0$, which implies that

$$\lim_{t\to\infty} n_I = f_I^{\text{sp}} \lim_{t\to\infty} n, \tag{41}$$

regardless of any condition other than $S_I^{\text{inj}} \equiv 0$. It can be noted from the equilibrium conditions for (9), i.e. $0 = -\frac{\bar{n}_I}{\bar{\tau}_I} + \bar{S}_I^{\text{sp}}$, and (10), i.e. $\bar{S}_I^{\text{sp}} = \frac{f_I^{\text{sp}}\bar{n}}{\bar{\tau}_I}$, that $\bar{n}_I = f_I^{\text{sp}}\bar{n}$, which is consistent with (41). Using (11) and (41), it is found that

$$\lim_{t\to\infty} n = \frac{3\lim_{t\to\infty} n_{\alpha} + 2\bar{n}_{\text{D}} + 2\bar{n}_{\text{T}}}{1 - f_I^{\text{sp}}(1 + Z_I)}. \tag{42}$$

So, if $\lim_{t\to\infty} n_{\alpha} = \bar{n}_{\alpha}$, n tends to its equilibrium value as well, and so does n_I. Then, it is necessary to inspect the terms on the right-hand side of (25). The first term, $-(\bar{n}_{\alpha} + \tilde{n}_{\alpha})/\tau_{\alpha} = -n_{\alpha}/\tau_{\alpha}$, decreases with an increase in n_{α}, and vice versa, it increases with a decrease in n_{α}. The second term, S_{α}, can be written as $S_{\alpha} = \bar{n}_{\text{D}}\bar{n}_{\text{T}}\langle\sigma v\rangle_{DT}$. To see the

dependence of S_α with n_α, it is necessary to analyze $\langle\sigma v\rangle_{DT}$, which is a positive, increasing function of T for the range of temperatures in which tokamaks operate [19]. Equation (11), together with (12), yields

$$T = \frac{E}{\frac{3}{2}n} = \frac{\bar{E}}{\frac{3}{2}(3n_\alpha + 2\bar{n}_\mathrm{D} + 2\bar{n}_\mathrm{T})}\left(1 - f_I^{\mathrm{sp}}(1+Z_I)\right), \tag{43}$$

where it has been used that $E = \bar{E}$, $n_\mathrm{D} = \bar{n}_\mathrm{D}$, $n_\mathrm{T} = \bar{n}_\mathrm{T}$, and $n_I = f_I^{\mathrm{sp}} n$ due to $S_I^{\mathrm{inj}} \equiv 0$. Therefore, increases in n_α imply decreases in T, which imply decreases in $\langle\sigma v\rangle_{DT}$ and in S_α. On the other hand, decreases in n_α imply increases in T, which imply increases in $\langle\sigma v\rangle_{\mathrm{DT}}$ and in S_α. Thus, due to the particular dependence of the right-hand-side terms of equation (25) with n_α, it is possible to write that

$$\frac{\mathrm{d}\tilde{n}_\alpha}{\mathrm{d}t} \propto -\tilde{n}_\alpha, \tag{44}$$

and it can be concluded that the $\tilde{n}_\alpha \to 0$ as $t \to \infty$. Then, n_α tends to $\bar{n}_\alpha$, n tends to $\bar{n}$, and n_I tends to $\bar{n}_I$, and the control objective is fully achieved.

Step 4: Fueling rate modulation ($\hat{\gamma}$ and $\tilde{n}$ control). By using isotopic fueling, the controller attempts to drive $\gamma \to \gamma^*$ to make $\tilde{E}$ asymptotically stable by exploiting the dependence of S_α on γ in (3). This γ^* value is obtained by solving the nonlinear equation

$$\gamma^*(1-\gamma^*) = \frac{\frac{\bar{E}}{\tau_\mathrm{E}} - P_\mathrm{Ohm} - P_\mathrm{aux} + P_\mathrm{rad} - K_{\gamma,1}\tilde{E}}{Q_\alpha (n_\mathrm{D}+n_\mathrm{T})^2 \langle\sigma v\rangle_{DT}}, \tag{45}$$

where $K_{\gamma,1} > 0$ is a design parameter. In this case, (29) reduces to $\mathrm{d}\tilde{E}/\mathrm{d}t = -\left(1/\tau_\mathrm{E} + K_{\gamma,1}\right)\tilde{E}$, and using the same Lyapunov function $V_{\tilde{E}} = \frac{1}{2}\tilde{E}^2 > 0$ as before, global asymptotical stability of $\tilde{E}$ is ensured because $\dot{V}_{\tilde{E}} = -\left(1/\tau_\mathrm{E} + K_{\gamma,1}\right)\tilde{E}^2 < 0$. For stability analysis, it is convenient to define $\hat{\gamma} \triangleq \gamma - \gamma^*$ since making $\hat{\gamma} \to 0$ is equivalent to making $\gamma \to \gamma^*$. Taking $S_\mathrm{T}^{\mathrm{inj}}$ as

$$S_\mathrm{T}^{\mathrm{inj,unsat}} = \frac{\gamma[f_{\mathrm{eff}}(S_\mathrm{D}^R + S_\mathrm{T}^R) - 2S_\alpha + S_\mathrm{D}^{\mathrm{inj,unsat}}] + S_\alpha - f_{\mathrm{eff}}S_\mathrm{T}^R + v}{1-\gamma}, \tag{46}$$

and using the definition for $\hat{\gamma}$ and (23), it is possible to write

$$\frac{\mathrm{d}\hat{\gamma}}{\mathrm{d}t} = \gamma(1-\gamma)\left(\frac{1}{\tau_\mathrm{D}} - \frac{1}{\tau_\mathrm{T}}\right) + \frac{v}{n_\mathrm{D}+n_\mathrm{T}} + \frac{\mathrm{d}\gamma^*}{\mathrm{d}t}. \tag{47}$$

By taking

$$v = -(n_\mathrm{D}+n_\mathrm{T})\left[\gamma(1-\gamma)\frac{1}{\tau_\mathrm{D}} + \frac{\gamma^2-\gamma^*}{\tau_\mathrm{T}} + K_{\gamma,2}\hat{\gamma} + \frac{\mathrm{d}\gamma^*}{\mathrm{d}t}\right], \tag{48}$$

where $K_{\gamma,2} > 0$ is a design parameter, it is found that $\mathrm{d}\hat{\gamma}/\mathrm{d}t = -\left(1/\tau_\mathrm{T} + K_{\gamma,2}\right)\hat{\gamma}$. Then, using $V_{\hat{\gamma}} = \frac{1}{2}\hat{\gamma}^2$, it is found that $\dot{V}_{\hat{\gamma}} = -\left(1/\tau_\mathrm{T} + K_{\gamma,2}\right)\hat{\gamma}^2 < 0$. Thus, global asymptotical stability of $\hat{\gamma}$ is ensured. Taking $S_\mathrm{D}^{\mathrm{inj}}$ as

$$S_\mathrm{D}^{\mathrm{inj,unsat}} = \frac{n_\mathrm{D}}{\tau_\mathrm{D}} + \frac{n_\mathrm{T}}{\tau_\mathrm{T}} - f_{\mathrm{eff}}(S_\mathrm{D}^R + S_\mathrm{T}^R) + 2S_\alpha - S_\mathrm{T}^{\mathrm{inj,unsat}} + w, \tag{49}$$

and using (22), it is possible to write

$$\frac{\mathrm{d}\tilde{n}}{\mathrm{d}t} = 3\left(-\frac{n_\alpha}{\tau_\alpha} + S_\alpha\right) + (1+Z_I)\left(-\frac{n_I}{\tau_I} + S_I^{\mathrm{inj}} + S_I^{\mathrm{sp}}\right) + 2w, \tag{50}$$

where $\tilde{n} \triangleq n - \bar{n}$. By taking

$$w = -\frac{1}{2}\left[3\left(-\frac{n_\alpha}{\tau_\alpha} + S_\alpha\right) + (1+Z_I)\left(-\frac{n_I}{\tau_I} + S_I^{\mathrm{inj}} + S_I^{\mathrm{sp}}\right) + K_n\tilde{n}\right], \tag{51}$$

where $K_n > 0$ is a design parameter, it is found that $\mathrm{d}\tilde{n}/\mathrm{d}t = -K_n\tilde{n}$. Using $V_{\tilde{n}} = \frac{1}{2}\tilde{n}^2$ ensures global asymptotical stability of $\tilde{n}$ because $\dot{V}_{\tilde{n}} = -K_n\tilde{n}^2 < 0$. Solving (46) and (49) for $S_\mathrm{D}^{\mathrm{inj,unsat}}$ and $S_\mathrm{T}^{\mathrm{inj,unsat}}$ yields

$$S_\mathrm{D}^{\mathrm{inj,unsat}} = (1-\gamma)\left(\frac{n_\mathrm{D}}{\tau_\mathrm{D}} + \frac{n_\mathrm{T}}{\tau_\mathrm{T}} + w\right) + S_\alpha - f_{\mathrm{eff}}S_\mathrm{D}^R - v, \tag{52}$$

$$S_\mathrm{T}^{\mathrm{inj,unsat}} = \gamma\left(\frac{n_\mathrm{D}}{\tau_\mathrm{D}} + \frac{n_\mathrm{T}}{\tau_\mathrm{T}} + w\right) + S_\alpha - f_{\mathrm{eff}}S_\mathrm{T}^R + v. \tag{53}$$

The stabilizing values for $S_{\text{D-line}}^{\mathrm{inj}}$ and $S_{\text{DT-line}}^{\mathrm{inj}}$ are obtained from solving (16) and (17) together with (52) and (53), and are given by

$$S_{\text{D-line}}^{\mathrm{inj,unsat}} = \frac{1}{\gamma_{\text{DT-line}}^{\mathrm{nom}} - \gamma_{\text{D-line}}^{\mathrm{nom}}}\left[\gamma_{\text{DT-line}}^{\mathrm{nom}}(1-\gamma)\left(\frac{n_\mathrm{D}}{\tau_\mathrm{D}} + \frac{n_\mathrm{T}}{\tau_\mathrm{T}} + w\right) - \gamma_{\text{D-line}}^{\mathrm{nom}}\gamma\left(\frac{n_\mathrm{D}}{\tau_\mathrm{D}} + \frac{n_\mathrm{T}}{\tau_\mathrm{T}} + w\right) + (\gamma_{\text{DT-line}}^{\mathrm{nom}} - \gamma_{\text{D-line}}^{\mathrm{nom}})\left(S_\alpha - f_{\mathrm{eff}}(S_\mathrm{D}^R + S_\mathrm{T}^R)\right) - v(\gamma_{\text{DT-line}}^{\mathrm{nom}} + \gamma_{\text{D-line}}^{\mathrm{nom}})\right], \tag{54}$$

$$S_{\text{DT-line}}^{\mathrm{inj,unsat}} = \frac{1}{\gamma_{\text{DT-line}}^{\mathrm{nom}} - \gamma_{\text{D-line}}^{\mathrm{nom}}}\left[(\gamma_{\text{DT-line}}^{\mathrm{nom}} - 1)(1-\gamma)\left(\frac{n_\mathrm{D}}{\tau_\mathrm{D}} + \frac{n_\mathrm{T}}{\tau_\mathrm{T}} + w\right) + (\gamma_{\text{DT-line}}^{\mathrm{nom}} - 1)(S_\alpha - f_{\mathrm{eff}}S_\mathrm{D}^R - v) + (1 - \gamma_{\text{D-line}}^{\mathrm{nom}})\gamma\left(\frac{n_\mathrm{D}}{\tau_\mathrm{D}} + \frac{n_\mathrm{T}}{\tau_\mathrm{T}} + w\right) + (1 - \gamma_{\text{D-line}}^{\mathrm{nom}})(S_\alpha - f_{\mathrm{eff}}S_\mathrm{T}^R + v)\right]. \tag{55}$$

Equations (54) and (55) are the nominal control laws for $S_{\text{DT-line}}^{\mathrm{inj}}$ and $S_{\text{D-line}}^{\mathrm{inj}}$, respectively, when Step 4 is activated. If the saturation limits $S_{\text{D-line}}^{\mathrm{inj,max}}$, $S_{\text{D-line}}^{\mathrm{inj,min}}$, $S_{\text{DT-line}}^{\mathrm{inj,max}}$, and $S_{\text{DT-line}}^{\mathrm{inj,min}}$ are reached, then the controller keeps $S_{\text{D-line}}^{\mathrm{inj}}/S_{\text{DT-line}}^{\mathrm{inj}}$ at the saturation limit that has been violated (i.e. same procedure as in Step 3). The stability of the $\tilde{E}$, $\tilde{n}$, and/or $\hat{\gamma}$ cannot be ensured in this case until the controller recovers from the saturation limits. Again, this is not a problem of the control algorithm but just a natural limitation imposed by the available actuation capability. However, in this case, impurity injection is activated for $\tilde{E}$ regulation (Step 5), as long as $n \leqslant 2f_{\mathrm{GW}}n_{\mathrm{GW}}$. If $n > 2f_{\mathrm{GW}}n_{\mathrm{GW}}$, impurity injection is never used, as it always increases n.

Finally, by following arguments similar to those used for Step 3, it can be shown that, if $\tilde{E}$, $\tilde{n}$, and $\tilde{\gamma}$ are driven to zero,

i.e. if $E = \bar{E}$, $n = \bar{n}$, and $\gamma = \bar{\gamma}$, then $\tilde{n}_\alpha$ and $\tilde{n}_I$ are also driven to zero as $t \to \infty$ provided that $S_I^{\text{inj}} \equiv 0$, and the control objective is fully achieved.

Step 5: Impurity injection. By using impurity injection, the controller attempts to drive $n_I \to n_I^*$ such that the $\tilde{E}$ evolution is asymptotically stable by exploiting the dependence of P_{rad} on n_I. This n_I^* value is obtained by solving the nonlinear equation

$$P_{\text{rad}}(n_I^*) = -\frac{\bar{E}}{\tau_{\text{E}}^{\min}} + P_\alpha^{\min} + P_{\text{Ohm}} + P_{\text{aux}}^{\min} + K_{n_I}\tilde{E}, \quad (56)$$

where $K_{n_I} > 0$ is a design parameter, and $P_\alpha^{\min}$ is the α heating achieved by isotopic fueling. Note that $P_{\text{aux}} = P_{\text{aux}}^{\min}$, $\tau_{\text{E}} = \tau_{\text{E}}^{\min}$, and $P_\alpha = P_\alpha^{\min}$, which means that impurity injection is used only when the combination of auxiliary power modulation (Step 1), in-vessel coil-current modulation (Step 2) and isotopic fueling (Step 3) is not enough to asymptotically stabilize $\tilde{E}$. In this case, (29) reduces to $\mathrm{d}\tilde{E}/\mathrm{d}t = -\left(1/\tau_{\text{E}}^{\min} + K_{n_I}\right)\tilde{E}$. By using $V_{\tilde{E}} = \frac{1}{2}\tilde{E}^2 > 0$ as before, global asymptotical stability of $\tilde{E}$ is ensured because $\dot{V}_{\tilde{E}} = -\left(1/\tau_{\text{E}}^{\min} + K_{n_I}\right)\tilde{E}^2 < 0$. It is convenient to define $\hat{n}_I \triangleq n_I - n_I^*$ for stability analysis since making $\hat{n}_I \to 0$ is equivalent to making $n_I \to n_I^*$. By using both this definition and (9), and by taking S_I^{inj} equal to

$$S_I^{\text{inj,unsat}} = \frac{n_I^*}{\tau_I} - S_I^{\text{sp}} - K_I\hat{n}_I + \frac{\mathrm{d}n_I^*}{\mathrm{d}t}, \quad (57)$$

where $K_I > 0$ is a design parameter, it is possible to write $\mathrm{d}\hat{n}_I/\mathrm{d}t = -\left(1/\tau_I + K_I\right)\hat{n}_I$. Taking $V_{\hat{n}_I} = \frac{1}{2}\hat{n}_I^2$, it is found that $\dot{V}_{\hat{n}_I} = -(1/\tau_I + K_I)\hat{n}_I^2 < 0$, which implies $\hat{n}_I \to 0$. Therefore, it can be ensured that $n_I \to n_I^*$ and $\tilde{E} \to 0$. Equation (57) is the control law for S_I^{inj}. Because of the upper saturation limit that exists for S_I^{inj}, denoted as $S_I^{\text{inj,max}}$ (note that $S_I^{\text{inj,min}} \equiv 0$), $\tilde{E} \to 0$ cannot be guaranteed until after the controller recovers from saturation.

4.2. Robust control law ($\delta_{\text{D-line}} \neq 0$, $\delta_{\text{DT-line}} \neq 0$)

The control laws obtained for the nominal system are robustified in this section for the uncertain system ($\delta_{\text{D-line}} \neq 0$, $\delta_{\text{DT-line}} \neq 0$) by following a Lyapunov redesign approach (see appendix B). The robust controller uses the same order and logic followed by the nominal controller for the activation of the actuators. Because the uncertainties are found in the $n_{\text{D}} - n_{\text{T}}$ balance equations, or alternatively, in the $n - \gamma$ balance equations, the control laws for auxiliary power modulation, in-vessel coil-current modulation, and controlled impurity injection do not need to be modified. On the other hand, the control laws for $S_{\text{D-line}}^{\text{inj}}$ and $S_{\text{DT-line}}^{\text{inj}}$, either controlling $\tilde{n}_{\text{D}}$ and $\tilde{n}_{\text{T}}$ (37) and (38), or controlling $\tilde{E}$ (through $\hat{\gamma}$) and $\tilde{n}$ (54) and (55), need to be modified to make them robust against the model uncertainties. Then, only Steps 3 and 4 need to be considered for redesign.

Step 3: Robust fueling rate modulation ($\tilde{n}_{\text{D}}$ and $\tilde{n}_{\text{T}}$ Control). Equations (26) and (27) can be written in matrix form as

$$\begin{bmatrix}\dot{\tilde{n}}_{\text{D}} \\ \dot{\tilde{n}}_{\text{T}}\end{bmatrix} = f + G\left[u + \delta\right], \quad (58)$$

where

$$f = \begin{bmatrix} -\frac{\bar{n}_{\text{D}}}{\tau_{\text{D}}} - \frac{\tilde{n}_{\text{D}}}{\tau_{\text{D}}} + S_{\text{D}}^R - S_\alpha \\ -\frac{\bar{n}_{\text{D}}}{\tau_{\text{T}}} - \frac{\tilde{n}_{\text{T}}}{\tau_{\text{T}}} + S_{\text{T}}^R - S_\alpha \end{bmatrix}, \quad (59)$$

$$G = \begin{bmatrix} 1 - \gamma_{\text{DT-line}}^{\text{nom}} & 1 - \gamma_{\text{D-line}}^{\text{nom}} \\ \gamma_{\text{DT-line}}^{\text{nom}} & \gamma_{\text{D-line}}^{\text{nom}} \end{bmatrix}, \quad (60)$$

$$u = \begin{bmatrix} S_{\text{DT-line}}^{\text{inj}} \\ S_{\text{D-line}}^{\text{inj}} \end{bmatrix}, \quad (61)$$

$$\delta = G^{-1}\begin{bmatrix} -(\delta_{\text{DT-line}}S_{\text{DT-line}}^{\text{inj}} + \delta_{\text{D-line}}S_{\text{D-line}}^{\text{inj}}) \\ \delta_{\text{DT-line}}S_{\text{DT-line}}^{\text{inj}} + \delta_{\text{D-line}}S_{\text{D-line}}^{\text{inj}} \end{bmatrix}. \quad (62)$$

The nominal control law for $\tilde{n}_{\text{D}} - \tilde{n}_{\text{T}}$, (37) and (38), is denoted by ψ_n. For the nominal $\tilde{n}_{\text{D}} - \tilde{n}_{\text{T}}$ subsystem, given by (58) with $\delta = 0$, it has been shown that $u = \psi_n$ is a stabilizing control law, i.e. the Lyapunov function $V_{\tilde{n}_{\text{DT}}} = V_{\tilde{n}_{\text{D}}} + V_{\tilde{n}_{\text{T}}} = \frac{1}{2}\tilde{n}_{\text{D}}^2 + \frac{1}{2}\tilde{n}_{\text{T}}^2$ yields $\dot{V}_{\tilde{n}_{\text{DT}}} = -\left(\frac{1}{\tau_D} + K_D\right)\tilde{n}_{\text{D}}^2 - \left(\frac{1}{\tau_T} + K_T\right)\tilde{n}_{\text{T}}^2$, which is strictly negative for all $\tilde{n}_{\text{D}}, \tilde{n}_{\text{T}} \neq 0$. A control law

$$u = \psi_n + v_{\text{rob}} \quad (63)$$

is now sought for the uncertain $\tilde{n}_{\text{D}} - \tilde{n}_{\text{T}}$ subsystem, given by (58) with $\delta \neq 0$, where v_{rob} is the part to be designed for robustness. Using a Lyapunov-redesign approach [22], v_{rob} is taken as

$$v_{\text{rob}} = \begin{cases} -\frac{\kappa_0\|\psi_n\|_2}{1-\kappa_0}\frac{w_{\text{rob}}}{\|w_{\text{rob}}\|_2} \text{ if } \kappa_0\|\psi_n\|_2\|w_{\text{rob}}\|_2 \geqslant \epsilon, \\ -\left(\frac{\kappa_0\|\psi_n\|_2}{1-\kappa_0}\right)^2\frac{w_{\text{rob}}}{\epsilon} \text{ if } \kappa_0\|\psi_n\|_2\|w_{\text{rob}}\|_2 < \epsilon, \end{cases} \quad (64)$$

where ϵ is a small positive design parameter that is needed to prevent a potential singularity of the control law at $\tilde{n}_{\text{D}} = \tilde{n}_{\text{T}} \equiv 0$, and w_{rob} is given by $w_{\text{rob}}^T = [\frac{\partial V_{\tilde{n}_{DT}}}{\partial \tilde{n}_{\text{D}}}, \frac{\partial V_{\tilde{n}_{DT}}}{\partial \tilde{n}_{\text{T}}}]G$, where $\kappa_0 = \sqrt{2(\delta_{\text{DT-line}}^{\max})^2 + (\delta_{\text{D-line}}^{\max})^2}/|\gamma_{\text{DT-line}}^{\text{nom}} - \gamma_{\text{D-line}}^{\text{nom}}|$ is a positive constant that is obtained by finding a bound to δ of the form $\|\delta(\psi_n + v_{\text{rob}})\|_2 \leqslant \kappa_0(\|\psi_n\|_2 + \|v_{\text{rob}}\|_2)$. This bound can be relatively easily obtained by using the triangular and the Cauchy–Schwarz inequalities. The modified control laws (63) and (64) do not assure that $\tilde{n}_{\text{D}} \to 0$ and $\tilde{n}_{\text{T}} \to 0$ in time, but they guarantee that $|\tilde{n}_D|$ and $|\tilde{n}_{\text{T}}|$ are bounded by class $\mathcal{K}$ functions of ϵ[1]. Therefore, it is critical to carefully choose ϵ so that it is small enough. Finally, using similar arguments to those used for the nominal system, it can be shown that if $\tilde{E}$ is driven to zero, $|\tilde{n}_\alpha|$ and $|\tilde{n}_I|$ are also bounded by class $\mathcal{K}$ functions of ϵ provided that $S_I^{\text{inj}} \equiv 0$.

Step 4: Robust fueling rate modulation ($\hat{\gamma}$ and $\tilde{n}$ control). Equations (30) and (31) can be written in matrix form as

[1] A continuous function $f(x)$ is said to be a class $\mathcal{K}$ function if: (1) it is a strictly increasing function of x, and (2) $f(0) = 0$.

$$\begin{bmatrix}\dot{\tilde{n}}\\ \dot{\hat{\gamma}}\end{bmatrix} = f^\star + G^\star\left[u+\delta^\star\right], \tag{65}$$

where

$$f^\star = \begin{bmatrix} f_1^\star \\ f_2^\star \end{bmatrix}, \tag{66}$$

$$f_1^\star = 3\left[-\frac{n_\alpha}{\tau_\alpha}+S_\alpha\right] + \left(3n_\alpha + (1+Z_I)\,n_I - n\right)\left(\frac{1-\gamma}{\tau_\mathrm{D}}+\frac{\gamma}{\tau_\mathrm{T}}\right) + 2f_\mathrm{eff}\left(S_\mathrm{D}^R+S_\mathrm{T}^R\right) - 4S_\alpha + (1+Z_I)\left[-\frac{n_I}{\tau_I}+S_I^\mathrm{sp}\right], \tag{67}$$

$$f_2^\star = \gamma(1-\gamma)\left(\frac{1}{\tau_\mathrm{D}}-\frac{1}{\tau_\mathrm{T}}\right) + \frac{2}{n-3n_\alpha-(1+Z_I)\,n_I}\left\{f_\mathrm{eff}S_\mathrm{T}^R - S_\alpha - \gamma\left[f_\mathrm{eff}\left(S_\mathrm{D}^R+S_\mathrm{T}^R\right)-2S_\alpha\right]\right\}, \tag{68}$$

$$G^\star = \begin{bmatrix} 2 & 2 \\ 2\frac{\gamma_{\mathrm{DT\text{-}line}}^\mathrm{nom}-\gamma}{n-3n_\alpha-(1+Z_I)n_I} & 2\frac{\gamma_{\mathrm{D\text{-}line}}^\mathrm{nom}-\gamma}{n-3n_\alpha-(1+Z_I)n_I} \end{bmatrix}, \tag{69}$$

$$\delta^\star = (G^\star)^{-1}\begin{bmatrix} 0 \\ 2\frac{\delta_{\mathrm{DT\text{-}line}}S_{\mathrm{DT\text{-}line}}^\mathrm{inj}}{n-3n_\alpha-(1+Z_I)n_I} + 2\frac{\delta_{\mathrm{D\text{-}line}}S_{\mathrm{D\text{-}line}}^\mathrm{inj}}{n-3n_\alpha-(1+Z_I)n_I} \end{bmatrix}. \tag{70}$$

The nominal control law for $\hat{\gamma}-\tilde{n}$ (isotopic fueling), (54) and (55), is denoted by $\psi_n^\star$. For the nominal $\tilde{n}_D-\hat{\gamma}$ subsystem, given by (65) with $\delta=0$, it has been shown that $u=\psi_n^\star$ is a stabilizing control law, i.e. the Lyapunov function $V_{\tilde{n},\hat{\gamma}} = V_{\tilde{n}}+V_{\hat{\gamma}} = \frac{1}{2}\tilde{n}^2+\frac{1}{2}\hat{\gamma}^2$ yields $\dot{V}_{\tilde{n},\hat{\gamma}} = -K_n\tilde{n}_\mathrm{D}^2 - \left(\frac{1}{\tau_\mathrm{T}}+K_{\gamma,2}\right)\hat{\gamma}^2$, which is strictly negative for all $\tilde{n}_\mathrm{D},\hat{\gamma}\neq 0$. A control law

$$u = \psi_n^\star + v_\mathrm{rob}^\star, \tag{71}$$

is now sought for the uncertain $\tilde{n}_\mathrm{D}-\hat{\gamma}$ subsystem, given by (65) with $\delta\neq 0$, where $v_\mathrm{rob}^\star$ is the part to be designed for robustness. Using a Lyapunov-redesign approach [22], $v_\mathrm{rob}^\star$ is taken as

$$v_\mathrm{rob}^\star = \begin{cases} -\frac{\kappa_0^\star\|\psi_n^\star\|_2}{1-\kappa_0^\star}\frac{w_\mathrm{rob}^\star}{\|w_\mathrm{rob}^\star\|_2} & \text{if } \kappa_0^\star\|\psi_n^\star\|_2\|w_\mathrm{rob}^\star\|_2 \geqslant \epsilon^\star, \\ -\left(\frac{\kappa_0^\star\|\psi_n^\star\|_2}{1-\kappa_0^\star}\right)^2\frac{w_\mathrm{rob}^\star}{\epsilon^\star} & \text{if } \kappa_0^\star\|\psi_n^\star\|_2\|w_\mathrm{rob}^\star\|_2 < \epsilon^\star, \end{cases} \tag{72}$$

where $\epsilon^\star$ is a small positive design parameter that is needed to prevent a potential singularity of the control law at $\tilde{n}=\hat{\gamma}\equiv 0$, and $w_\mathrm{rob}^\star$ is given by $(w_\mathrm{rob}^\star)^T = [\frac{\partial V_{\tilde{n},\hat{\gamma}}}{\partial\tilde{n}}, \frac{\partial V_{\tilde{n},\hat{\gamma}}}{\partial\hat{\gamma}}]G^\star$, where $\kappa_0^\star=\kappa_0$ is a constant that is obtained by finding a bound to $\delta^\star$ of the form $\|\delta^\star(\psi_n^\star+v_\mathrm{rob}^\star)\|_2 \leqslant \kappa_0^\star(\|\psi_n^\star\|_2+\|v_\mathrm{rob}^\star\|_2)$. As in the case for Step 3, this bound can be relatively easily obtained by using the triangular and the Cauchy–Schwarz inequalities. The modified control laws (71) and (72) do not assure that $\tilde{n}\to 0$ and $\hat{\gamma}\to 0$ in time, but they guarantee that $|\tilde{n}|$ and $|\hat{\gamma}|$ are bounded by class $\mathcal{K}$ functions of $\epsilon^\star$. As before, ϵ^* must be chosen small enough. Finally, following similar arguments as before, it can be shown that $|\tilde{n}_\alpha|$ and $|\tilde{n}_I|$ are also bounded by class $\mathcal{K}$ functions of $\epsilon^\star$ if $\tilde{E}$ is driven to zero and provided that $S_I^\mathrm{inj}\equiv 0$.

A summary of the variables employed in this section is shown in table 3.

5. Simulation study

The performance of the proposed controller is tested in this section for two different scenarios. In the first scenario, a first operating point with high density is used to test the controller performance when isotopic fueling (i.e. $\tilde{n}-\hat{\gamma}$ control) is employed to regulate the plasma density n, while a second operating point with lower density is used to test the controller performance when switching between isotopic fueling and $\tilde{n}_\mathrm{D}-\tilde{n}_\mathrm{T}$ control. No recycling and a relatively small amount of impurities are considered in this first simulation case. In the second scenario, operating points with lower density are chosen so that $\tilde{n}_\mathrm{D}-\tilde{n}_\mathrm{T}$ control is used during most of the simulation, only using isotopic fueling as a backup to decrease the plasma energy when needed. Also, recycling effects are included and a higher amount of impurities is introduced in this second simulation case in order to test the controller in a more demanding situation. In both scenarios, perturbations in the D–T concentrations of the fueling lines are emulated to test the robustness of the controller under the presence of the uncertainties $\delta_\mathrm{DT\text{-}line}$ and $\delta_\mathrm{D\text{-}line}$. It is very important to emphasize that such perturbations in the D–T concentrations with respect to the nominal case are totally unknown to the controller during the simulations studies. The saturation limits imposed are shown in table 4. Also, the following parameters are used: $k_\alpha=5$, $k_\mathrm{D}=2.5$, $k_\mathrm{T}=2.5$, and $k_I=8$.

5.1. Scenario 1

In this first scenario, recycling effects are neglected ($f_\mathrm{eff}=0$), and it is considered that the content of impurities in the plasma is relatively low ($f_I^\mathrm{sp}=0.005$). Also, only beryllium impurities are considered ($Z_I=4$), and the H-factor without activation of the in-vessel coils is taken as $H_{\mathrm{H},0}=1.1$. Regarding the uncertainties (see equations (18) and (19)), a constant negative 30% drop in the T concentration of the D–T pellet injector is emulated during the whole simulation, i.e. $\delta_\mathrm{DT\text{-}line}=-0.3$, whereas no T is assumed in the D pellet injector (as in the nominal case), i.e. $\delta_\mathrm{D\text{-}line}=0$. Firstly, the controller attempts to regulate the system around a first operating point defined by $\bar{T}=10$ keV, $\bar{\beta}_N=2$, and $\bar{\gamma}=0.5$, from $t=0$ s until $t=50$ s. The simulation study starts from a perturbed initial condition with respect to this first equilibrium point (+20% in n_α, +30% in n_D, −10% in n_T, and +20% in E (no perturbation is introduced in n_I)). Secondly, at $t=50$ s, the controller attempts to drive the system to a different operating point defined by $\bar{T}=12$ keV, $\bar{\beta}_N=1.75$, and $\bar{\gamma}=0.45$. Finally, from $t=100$ s until $t=150$ s, the controller tries to drive the system back to the first operating point. Because the first operating point is characterized by a value of n which is close to the Greenwald

Table 3. Controller variables.

Symbol	Description	Type of variable
$\bar{(\cdot)}$	Equilibrium variable	Reference
$\tilde{(\cdot)}$	Deviation variable	Error
$P_{\text{aux}}^{\text{unsat}}$	Auxiliary power from control law	Control law variable
$I_{\text{coil}}^{\text{unsat}}$	In-vessel coil current from control law	Control law variable
$S_{\text{D/DT}-\text{line}}^{\text{inj,unsat}}$, $S_{\text{D/DT}-\text{line}}^{\text{inj,unsat}}$	D and DT pellet injection from control law	Control law variable
$S_I^{\text{inj,unsat}}$	Impurity injection rate from control law	Control law variable
$P_{\text{aux}}^{\text{max}}$, $P_{\text{aux}}^{\text{min}}$	Max/min P_{aux}	Saturation level
$I_{\text{coil}}^{\text{max}}$	Max in-vessel coil current	Saturation level
$S_{\text{D/DT}-\text{line}}^{\text{inj,max}}$, $S_{\text{D/DT}-\text{line}}^{\text{inj,min}}$	Max/min D and DT pellet injection rates	Saturation level
$S_I^{\text{inj,max}}$	Max impurity injection rate	Saturation level
K_P, $K_{\tau_{\text{E}}}$, K_{D}, K_{T}	Nominal controller gains	Design parameter
$K_{\gamma,1}$, $K_{\gamma,2}$, K_n, K_{n_I}, K_I	Nominal controller gains	Design parameter
f_{GW}	Greenwald density proximity constant	Design parameter
n_{GW}	Greenwald density	Intermediate variable
P^{min}	P with minimum P_{aux}	Intermediate variable
$\tau_{\text{E}}^{\text{min}}$	τ_{E} with minimum I_{coil}	Intermediate variable
$\hat{n}_I$	Deviation in n_I w.r.t. steady-state value	Intermediate variable
γ^*, $\hat{\gamma}$	γ and error for isotopic fueling	Intermediate variable
n_I^*, $\hat{n}_I$	n_I and error for impurity injection	Intermediate variable
$V_{(\cdot)}$	Lyapunov functions	Intermediate variable
f, G, u, δ	Matrices for $n_{\text{D}} - n_{\text{T}}$ uncertain model	Intermediate variable
$f^\star$, $G^\star$, u, $\delta^\star$	Matrices for $n - \gamma$ uncertain model	Intermediate variable
ψ_n, $\psi_n^\star$, v, w	Functions for nominal fueling control	Intermediate variable
v_{rob}, $v_{\text{rob}}^\star$, w_{rob}, $w_{\text{rob}}^\star$	Functions for robust fueling control	Intermediate variable
κ_0, $\kappa_0^\star$	Constants from bounds to δ and $\delta^\star$	Model parameter
ϵ, $\epsilon^\star$	Constants for robust fueling control	Design parameter

density limit, $f_{\text{GW}} = 0.8$ is taken so that n is regulated by isotopic fueling around such operating point in order to prevent instabilities related to too high density values.

Simulation results for the evolutions of β_N, n, γ, T, n_{D} and n_{T} together with their corresponding targets are shown in figure 3 for three different cases: (i) open loop (no control), (ii) closed loop under the nominal control law, (iii) closed loop under the robust control law. The inputs $S_{\text{D}}^{\text{inj}}$, $S_{\text{T}}^{\text{inj}}$,

Table 4. Actuator limits.

Symbol	Description	Value
$P_{\text{aux}}^{\text{max}}$	Maximum power	73 MW
$P_{\text{aux}}^{\text{min}}$	Minimum power	35 MW
$S_{\text{D}}^{\text{max}}$	Maximum D fueling rate	3×10^{19} m^{-3} s^{-1}
$\dot{S}_{\text{D}}^{\text{max}}$	Maximum D fueling ramp rate	3×10^{19} m^{-3} s^{-2}
$S_{\text{T}}^{\text{max}}$	Maximum T fueling rate	3×10^{19} m^{-3} s^{-1}
$\dot{S}_{\text{T}}^{\text{max}}$	Maximum T fueling ramp rate	3×10^{19} m^{-3} s^{-2}
$I_{\text{coil}}^{\text{max}}$	Maximum in-vessel coil current	4 kA

$S_{\text{D-line}}^{\text{inj}}$, $S_{\text{DT-line}}^{\text{inj}}$, I_{coil} and P_{aux} are shown in figure 4. In the case of nominal D–T fuel concentration, the reference actuator signals (red dashed) shown in figure 4 are designed to achieve in open loop the desired reference states (red dashed) shown in figure 3. However, in presence of the emulated bias in the T concentration of the D–T pellet injector, the variables evolve in open loop (black dotted) to values that are different from the desired references (red dashed) as shown in figure 3. Under the nominal control law, β_N is driven to the desired operating points during the whole simulation (see figure 3(*a*)), whereas n and T can only be driven to the first operating point; at $t = 50$ s, the nominal control law is unable to accurately drive n and T to the second operating point, and it is also unable to drive n and T back to the first operating point at $t = 100$ s (see figures 3(*b*) and (*d*)). Because $n > 2f_{\text{GW}}n_{\text{GW}}$ between $t = 0$ s and $t \approx 50$ s, and later between $t \approx 100$ s and $t \approx 150$ s, isotopic fueling is employed during those time intervals (figure 3(*b*)), while $\tilde{n}_{\text{D}} - \tilde{n}_{\text{T}}$ control is used between $t \approx 50$ s and $t \approx 100$ s. In open loop, n goes beyond the Greenwald stability limit, while the nominal and robust control laws avoid violating such limit. Still, the nominal control law cannot drive γ, n_{D} and n_{T} to the desired operating points during the entire simulation (see figures 3(*c*), (*e*) and (*f*)). On the other hand, the robust control law is able to successfully drive all the variables β_N, n, γ, T, n_{D} and n_{T} to the different operating points. Figure 4 shows that the robust control law can correct the drifts in the DT concentration of the pellet injectors even though they are unknown to the controller, and drives P_{aux}, $S_{\text{D}}^{\text{inj}}$ and $S_{\text{T}}^{\text{inj}}$ to their equilibrium values (see figures 4(*a*), (*b*) and (*f*)). It must be emphasized that $S_{\text{D-line}}^{\text{inj}}$ and $S_{\text{DT-line}}^{\text{inj}}$ are not expected to converge to their reference values due to the emulated bias. The in-vessel coils are utilized by both the nominal and robust control laws during the short periods of time in which P_{aux} is saturated to its minimum value, around $t = 0$ s and $t = 50$ s (see figures 4(*e*) and (*f*)). Impurity injection is not used at all by the controller due to the fact that, while isotopic fueling is employed, density limits are closed to be violated (i.e. $n > 2f_{\text{GW}}n_{\text{GW}}$).

5.2. Scenario 2

In this second scenario, intense recycling effects ($f_{\text{eff}} = 0.3$, $f_{\text{ref}} = 0.65$, $R_{\text{eff}} = 0.85$, $\gamma_{\text{PFC}} = 0.5$) and a relatively high content of impurities in the plasma ($f_I^{\text{sp}} = 0.05$) are considered.

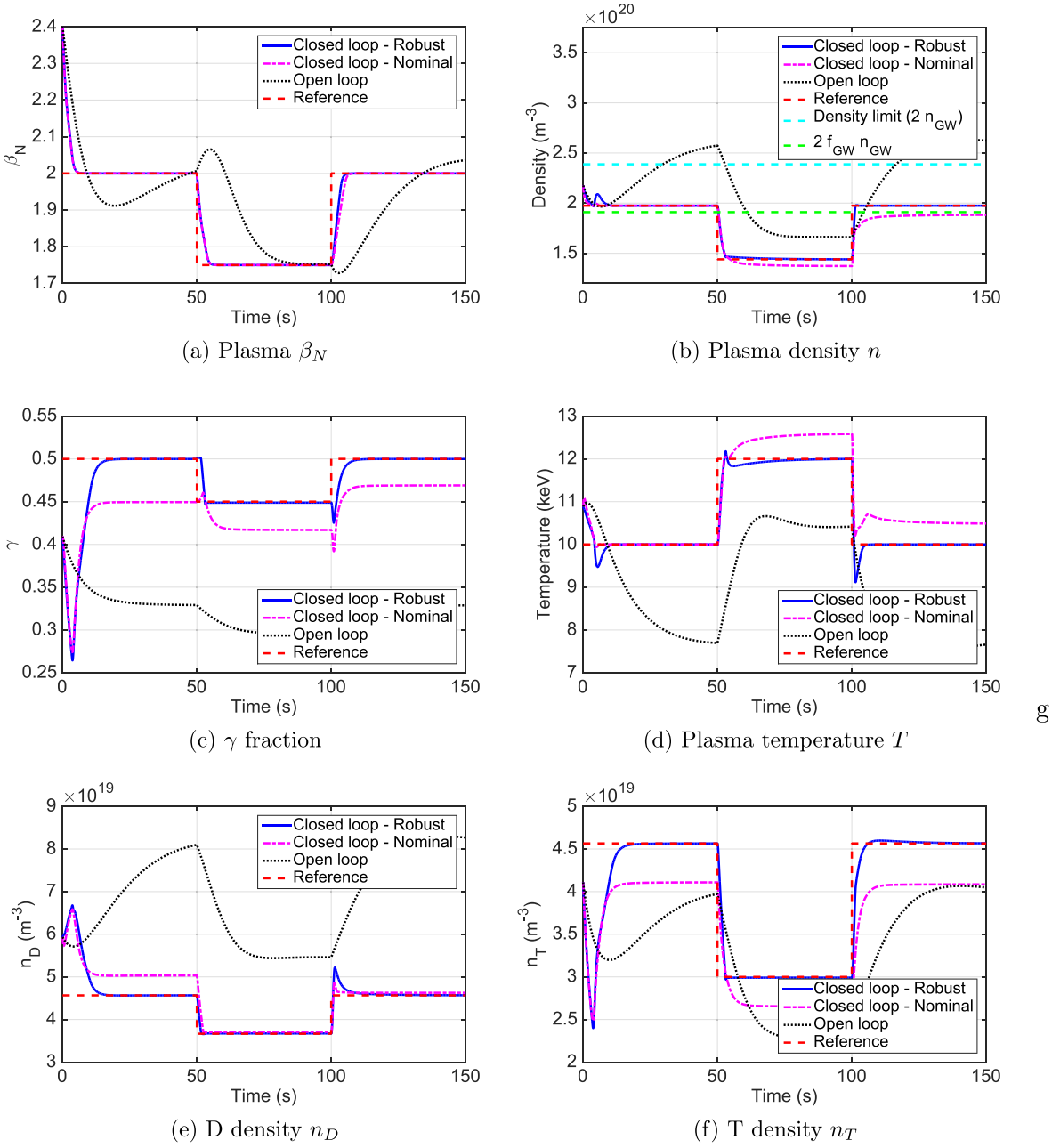

(a) Plasma β_N (b) Plasma density n

(c) γ fraction (d) Plasma temperature T

(e) D density n_D (f) T density n_T

Figure 3. Time evolutions for β_N, n, γ, T, n_{D}, and n_{T} in Scenario 1 under robust feedback control law (solid blue), nominal feedback control law (magenta dashed–dotted), and feedforward control law (black dotted), together with the reference signals (red dashed).

Also, impurities with higher atomic number are considered (carbon, $Z_I = 6$), and the H-factor without activation of the in-vessel coils is taken as $H_{\mathrm{H},0} = 1.2$. For a more demanding test of the controller, the uncertain terms $\gamma_{\text{D-line}}$ and $\gamma_{\text{DT-line}}$ (see equations (18) and (19)) vary in time as shown in figure 6(*h*). Firstly, the controller attempts to regulate the system around a first operating point defined by $\bar{T} = 10$ keV, $\bar{\beta}_N = 1.5$, and $\bar{\gamma} = 0.5$, from $t = 0$ s till $t = 50$ s. The simulation study starts from a perturbed initial condition with respect to the equilibrium ($+20\%$ in n_α, -10% in n_{D}, $+15\%$ in n_{T}, and $+20\%$ in E (again, no perturbation is introduced in n_I)). Secondly, at $t = 50$ s, the controller attempts to drive the system to a different operating point defined by $\bar{T} = 11$ keV, $\bar{\beta}_N = 1.4$, and $\bar{\gamma} = 0.45$. Finally, from $t = 100$ s until $t = 150$ s, the controller attempts to drive the system to a third operating point defined by $\bar{T} = 10.5$ keV, $\bar{\beta}_N = 1.6$, and $\bar{\gamma} = 0.5$. Because the density values that characterize these three operating points are substantially lower than in the first simulation scenario, regulation of n due to closeness to the Greenwald density limit is not considered as a priority in this case. A value of $f_{\mathrm{GW}} = 1$ is taken.

Simulation results for the evolutions of $\beta_N, n, \gamma, T, n_{\mathrm{D}}$ and n_{T} together with their corresponding targets are shown in figure 5 for three different cases: (i) open loop (no control), (ii) closed

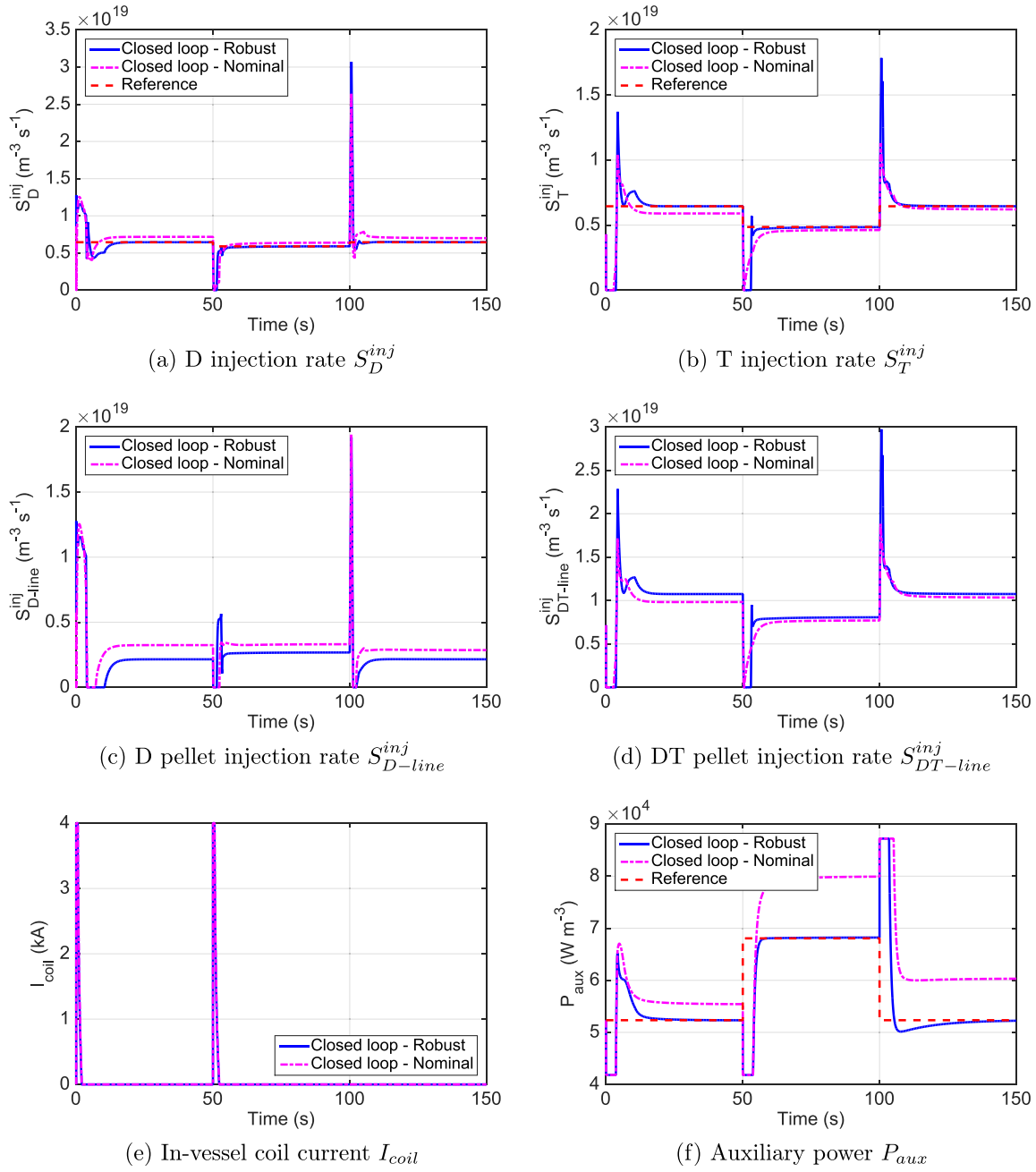

(a) D injection rate S_D^{inj} (b) T injection rate S_T^{inj}

(c) D pellet injection rate S_{D-line}^{inj} (d) DT pellet injection rate $S_{DT-line}^{inj}$

(e) In-vessel coil current I_{coil} (f) Auxiliary power P_{aux}

Figure 4. Time evolutions for $S_{\mathrm{D}}^{\mathrm{inj}}$, $S_{\mathrm{T}}^{\mathrm{inj}}$, $S_{\mathrm{D\text{-}line}}^{\mathrm{inj}}$, $S_{\mathrm{DT\text{-}line}}^{\mathrm{inj}}$, I_{coil}, and P_{aux} in Scenario 1 under robust (solid blue) and nominal (magenta dashed–dotted) control laws, together with the actuator reference (red dashed).

loop under the nominal control law, (iii) closed loop under the robust control law. The inputs $S_{\mathrm{D}}^{\mathrm{inj}}$, $S_{\mathrm{T}}^{\mathrm{inj}}$, $S_{\mathrm{D\text{-}line}}^{\mathrm{inj}}$, $S_{\mathrm{DT\text{-}line}}^{\mathrm{inj}}$, I_{coil} and P_{aux} are shown in figure 6 together with $\gamma_{\mathrm{D\text{-}line}}$ and $\gamma_{\mathrm{DT\text{-}line}}$. As in the previous simulation case, the reference actuator signals (red dashed) shown in figure 6 are designed to achieve in open loop the desired reference states (red dashed) shown in figure 5 for the case of nominal D–T fuel concentration. However, in presence of the emulated drifts in the T concentrations of both the D pellet injector and the D–T pellet injector, the variables evolve in open loop (black dotted) to values that are different from the desired references (red dashed) as shown in figure 5. Under the nominal control law, β_N is driven to the desired operating points during the whole simulation, and n_{D} is also successfully regulated, although with small constant drifts with respect to the desired targets (see figures 5(*a*) and (*e*)). However, the nominal control law cannot drive n, γ, T, and n_{T} to the desired operating points (see figures 5(*b*)–(*d*) and (*f*)). On the contrary, the robust control law is able to successfully drive all the variables β_N, n, γ, T, n_{D} and n_{T} to the different operating points. It is interesting to note that the high content

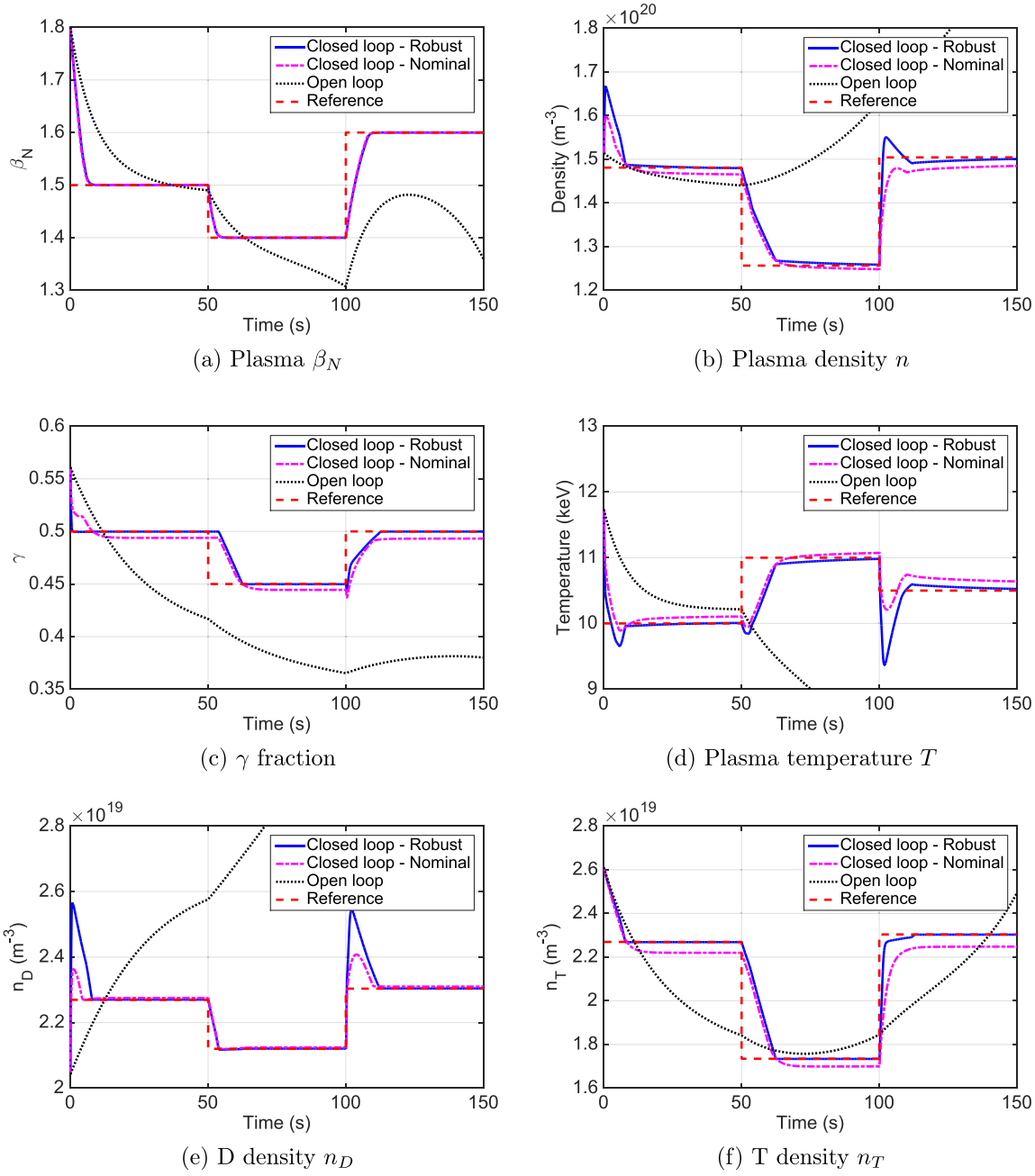

(a) Plasma β_N (b) Plasma density n

(c) γ fraction (d) Plasma temperature T

(e) D density n_D (f) T density n_T

Figure 5. Time evolutions for β_N, n, γ, T, n_{D}, and n_{T} in Scenario 2 under robust feedback control law (solid blue), nominal feedback control law (magenta dashed–dotted), and feedforward control law (black dotted), together with the reference signals (red dashed). .

of impurities and the recycling effects slow down the n and T evolutions when compared to those in Scenario 1, even though the robust controller still regulates both n and T successfully. Figure 6 shows how P_{aux}, $S_{\mathrm{D}}^{\mathrm{inj}}$ and $S_{\mathrm{T}}^{\mathrm{inj}}$ evolve to their equilibrium values both under the nominal and robust control laws (see figures 6(*a*), (*b*) and (*f*)). However, the $S_{\mathrm{D}}^{\mathrm{inj}}$ and $S_{\mathrm{T}}^{\mathrm{inj}}$ evolutions are slightly different, which has an important impact on the state evolution due to the highly nonlinear nature of the system. The in-vessel coils are utilized by both the nominal and robust control laws during the short periods of time in which P_{aux} is saturated to its minimum value, around $t = 0$ s and $t = 50$ s (see figures 6(*e*) and (*f*)). Impurity injection is used only at the beginning of the simulation during a few seconds, in order to reject the initial perturbation in E.

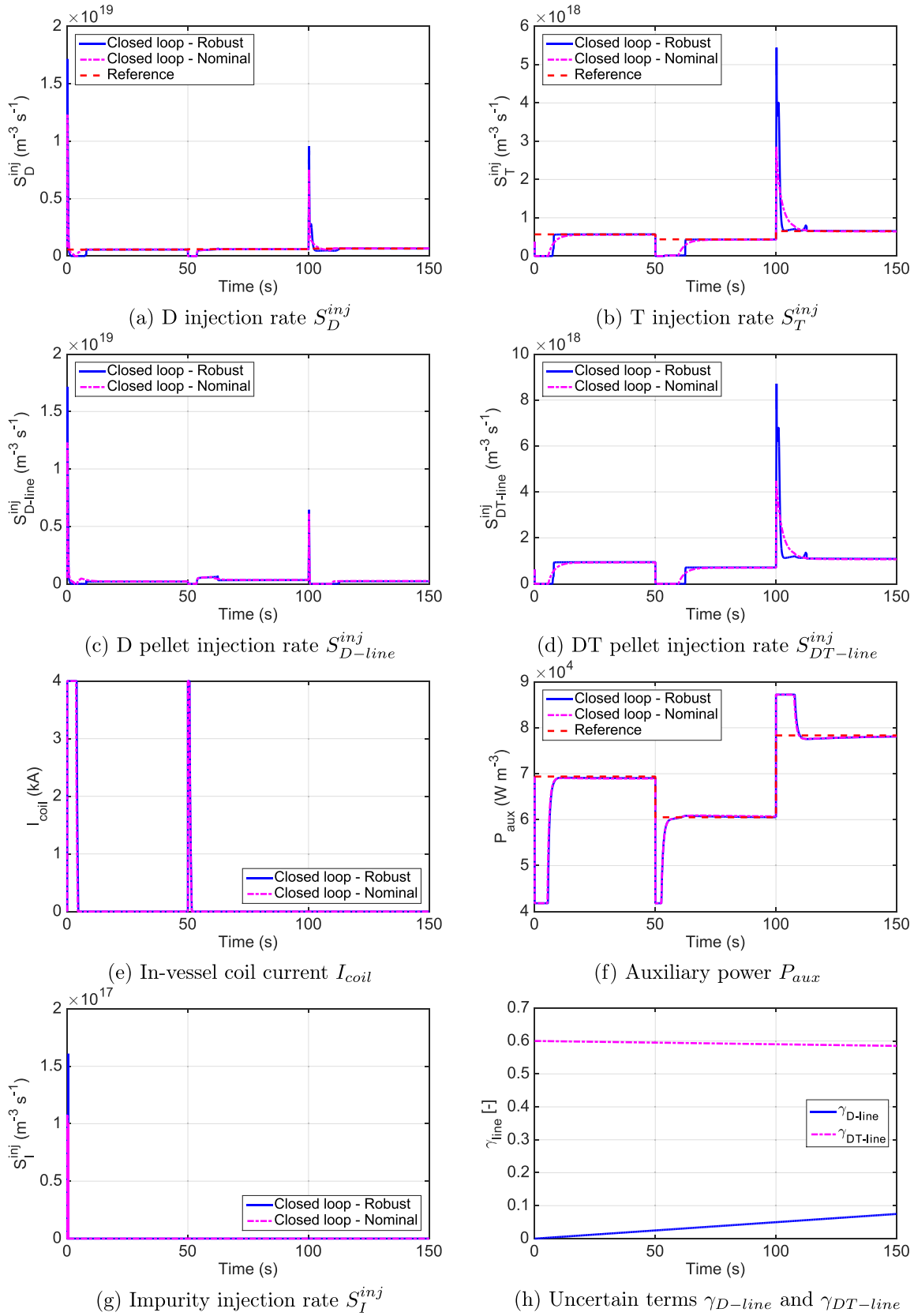

(a) D injection rate S_D^{inj} (b) T injection rate S_T^{inj}

(c) D pellet injection rate S_{D-line}^{inj} (d) DT pellet injection rate $S_{DT-line}^{inj}$

(e) In-vessel coil current I_{coil} (f) Auxiliary power P_{aux}

(g) Impurity injection rate S_I^{inj} (h) Uncertain terms γ_{D-line} and $\gamma_{DT-line}$

Figure 6. Time evolutions for $S_{\mathrm{D}}^{\mathrm{inj}}$, $S_{\mathrm{T}}^{\mathrm{inj}}$, $S_{\mathrm{D\text{-}line}}^{\mathrm{inj}}$, $S_{\mathrm{DT\text{-}line}}^{\mathrm{inj}}$, I_{coil}, P_{aux}, S_I^{inj}, $\gamma_{\mathrm{D\text{-}line}}$ and $\gamma_{\mathrm{DT\text{-}line}}$ in Scenario 2 under robust (solid blue) and nominal (magenta dashed–dotted) control laws, and actuator reference (red dashed).

6. Conclusions

A nonlinear, robust burn controller, which is capable of regulating the burning plasma around a desired equilibrium under the presence of large initial perturbations and uncertainties in the D–T concentration of the pellet injectors, has been presented. The controller can be used to drive the system between different operating points, since the control-design process avoids model linearization around a particular equilibrium. Moreover, the algorithm combines all feasible actuators available in tokamaks for burn control (auxiliary power, in-vessel coil current, fueling rates, and impurity injection) in a comprehensive, integrated control strategy, which allows for a higher flexibility when choosing the most appropriate actuation methods in different scenarios. For instance, the controller chooses isotopic fueling in scenarios in which disruptive density limits may be reached, whereas it chooses a more accurate D and T density control approach around operating points that are relatively far from disruptive density limits. The nonlinear control laws for the different actuators are given as analytical functions of the measured or estimated states, which makes this control approach much less computationally demanding than any possible real-time nonlinear optimization approach and also much more robust since it is immune to feasibility and convergence issues. The controller performance has been studied in simulations for two different scenarios. The simulation study suggests both that the D–T pellet-concentration variations play a crucial role in the burning plasma dynamics and that robust burn controllers are necessary to effectively overcome their negative impact in ITER.

A simplified zero-dimensional, nonlinear model is used in this work for control synthesis and simulation. Even though these models are approximate, they capture the primary dynamics of the burning plasma that is needed for the synthesis of a robust controller whose control objective is defined in terms of zero-dimensional quantities such as the overall fusion power. However, as one-dimensional fueling actuation models become more mature, steps towards control simulations based on one-dimensional models are necessary because while the control objective is zero-dimensional, the to-be-controlled system is indeed one-dimensional. Future work also requires the incorporation of the actuator and sensor dynamics in the control-design process. It is anticipated that the proposed burn-control algorithm will need to be augmented to handle lags and delays associated with the actuators and sensors possibly by the use of backstepping and prediction techniques.

Acknowledgments

This work was supported by the U.S. Department of Energy under contract DE-SC0010661.

Appendix A. Lyapunov theory basics

The Lyapunov stability theory is the basis of the controller design and stability proofs shown in this paper. Consider a nonlinear, autonomous system

$$\dot{x} = g(x,u), \tag{A.1}$$

where $x \in \mathbb{R}^n$ is the state vector, $u \in \mathbb{R}^p$ is the input vector, and $g : D \times \mathbb{R}^p \to \mathbb{R}^n$ is a nonlinear function. It is assumed that a control law $u = \psi_n(x)$ is known and set such that $g(x, \psi_n(x)) \triangleq f(x)$, and also that the resulting function $f : D \to \mathbb{R}^n$ is locally Lipschitz in the domain $D \subset \mathbb{R}^n$. It is said that $x = \bar{x}$ is an equilibrium of the system if

$$f(\bar{x}) = 0. \tag{A.2}$$

Without loss of generality, it is possible to use the change of variables $\tilde{x} = x - \bar{x}$ so that (A.1) can be rewritten as

$$\dot{\tilde{x}} = f(\tilde{x}), \tag{A.3}$$

which is a system with an equilibrium at the origin. It is necessary to define stability, asymptotical stability, and global asymptotical stability of an equilibrium. The equilibrium $\tilde{x} = 0$ of the system (A.3) is stable if, for each $\epsilon > 0$, there exists $\delta = \delta(\epsilon) > 0$ such that

$$\|\tilde{x}(0)\| < \delta \Rightarrow \|\tilde{x}(t)\| < \epsilon, \forall t \geqslant 0. \tag{A.4}$$

Such equilibrium is asymptotically stable if it is stable and δ can be found such that

$$\|\tilde{x}(0)\| < \delta \Rightarrow \lim_{t\to\infty} \tilde{x}(t) = 0, \tag{A.5}$$

and it is globally asymptotically stable if $\|\tilde{x}(0)\|$ can be taken arbitrarily large. The main Lyapunov theorem exploited in this work says that, if a function $V : \mathbb{R}^n \to \mathbb{R}^n$ can be found for the system (A.3) such that

$$V(0) = 0, \tag{A.6}$$

$$V(\tilde{x}) > 0, \forall \tilde{x} \neq 0, \tag{A.7}$$

$$\|\tilde{x}\| \to \infty \Rightarrow V(\tilde{x}) \to \infty, \tag{A.8}$$

$$\dot{V}(x) < 0, \forall x \neq 0, \tag{A.9}$$

then the equilibrium $\tilde{x} = 0$ is globally asymptotically stable. If condition (A.8) cannot be satisfied, globality cannot be claimed. In general, finding the function V, known as Lyapunov function, is a complicated problem. Typical candidates for Lyapunov functions are quadratic functions, $V = \tilde{x}^T P \tilde{x}$ ($P > 0$), such that $\dot{V} = -\tilde{x}^T Q \tilde{x}$ with $Q > 0$. A more detailed introduction to Lyapunov stability theory can be found in [22]. In this work, the control-design problem is not only finding the Lyapunov functions themselves, which are given by relatively simple quadratic functions, but also finding the stabilizing feedback laws $u = \psi_n(x)$ at the same time.

Appendix B. Lyapunov redesign basics

Lyapunov redesign is the technique employed in this work to design a robust, nonlinear controller. Consider a nonlinear, autonomous, uncertain system with the following shape

$$\dot{x} = f(x) + G(x)[u + \delta(x,u)], \tag{B.1}$$

where $x \in \mathbb{R}^n$ is the state vector, $u \in \mathbb{R}^p$ is the input vector, $\delta \in \mathbb{R}^p$ is the uncertainty vector, and $f : D \to \mathbb{R}^n$, $G : D \to \mathbb{R}^{n\times p}$ and $\delta : D \times \mathbb{R}^p \to \mathbb{R}^p$ are locally Lipschitz in x and u. It is assumed that a control law $u = \psi_n(x)$ and a Lyapunov function $V(x)$ have been found such that the origin of (B.1) is a globally asymptotically stable equilibrium in closed loop for the nominal system ($\delta = 0$). A control law $u = \psi_n + v$ is sought such that (B.1) is asymptotically stable when $\delta \neq 0$. The time derivative of V is given by

$$\dot{V} = \frac{\partial V}{\partial x}(f + G\psi_n) + \frac{\partial V}{\partial x}G\Big(v + \delta\Big), \tag{B.2}$$

where the dependence on x and u has been dropped to simplify notation. The term $\frac{\partial V}{\partial x}(f + G\psi_n)$ corresponds to the time derivative of V when the control law $u = \psi_n(x)$ is employed for the nominal system ($\delta \equiv 0$), which is negative by design. Therefore $\frac{\partial V}{\partial x}(f + G\psi_n) < -\alpha_c(\|x\|)$, where α_c is a class $\mathcal{K}$ function. Then, it is found that

$$\dot{V} < -\alpha_c(\|x\|) + \frac{\partial V}{\partial x}G\Big(v + \delta\Big). \tag{B.3}$$

The term v must be designed such that $\dot{V} < 0$, regardless of the value of δ. Using the Cauchy–Schwarz inequality, (B.3) can be rewritten as

$$\dot{V} < -\alpha_c(\|x\|) + \frac{\partial V}{\partial x}Gv + \left\|\frac{\partial V}{\partial x}G\right\|_2 \|\delta\|_2 . \tag{B.4}$$

If there exists a bound with the shape

$$\|\delta(x, \psi_n(x) + v)\|_2 \leqslant \kappa_0(\|\rho_c(x)\|_2 + \|v\|_2), \tag{B.5}$$

where $\kappa_0 < 1$ and $\rho_c : D \to \mathbb{R}^p$ is non-negative, then

$$\dot{V} < -\alpha_c(\|x\|) + \frac{\partial V}{\partial x}Gv + \left\|\frac{\partial V}{\partial x}G\right\|_2 \kappa_0(\|\rho_c\|_2 + \|v\|_2), \tag{B.6}$$

and if v is taken as

$$v = -\frac{\kappa_0 \|\rho_c\|_2}{1 - \kappa_0}\frac{\left(\frac{\partial V}{\partial x}G\right)^T}{\left\|\frac{\partial V}{\partial x}G\right\|_2}, \tag{B.7}$$

then

$$\frac{\partial V}{\partial x}Gv + \left\|\frac{\partial V}{\partial x}G\right\|_2 \kappa_0(\|\rho_c\|_2 + \|v\|_2) = 0, \tag{B.8}$$

and

$$\dot{V} < -\alpha_c(\|x\|). \tag{B.9}$$

Therefore, the origin of (B.1) is globally asymptotically stable under the control law $u = \psi_n + v$, with v given by (B.7), as long as a bound (B.5) can be found. However, a control law using (B.7) is undetermined at $\frac{\partial V}{\partial x}G = 0$. In order to avoid such problem, (B.7) is modified as

$$v = -\left(\frac{\kappa_0 \|\rho_c\|_2}{1 - \kappa_0}\right)^2 \frac{\left(\frac{\partial V}{\partial x}G\right)^T}{\epsilon}, \tag{B.10}$$

whenever $\kappa_0 \|\rho_c\|_2 \left\|\frac{\partial V}{\partial x}G\right\|_2 < \epsilon$, for some design parameter ϵ. The control law (B.7)–(B.10) does not ensure global asymptotical stability, but it does ensures that x is bounded by a class $\mathcal{K}$ function of ϵ [22]. Therefore, ϵ must be small in order to make the bound on x as small as possible, ensuring that x remains close to 0.

References

[1] Chaniotakis E., Freidberg J. and Cohn D. 1989 CIT burn control using auxiliary power modulation *Proc. 13th IEEE/NPSS Symp. Fusion Engineering* vol 1 (IEEE) pp 400–3
[2] Haney S. and Perkins L. 1989 Operating point selection and burn stability control for the International Thermonuclear Experimental Reactor *Proc. 13th IEEE/NPSS Symp. Fusion Engineering* vol 1 (IEEE) pp 396–9
[3] Hui W., Fischbach K., Bamieh B.A. and Miley G.H. 1993 Effectiveness and constraints of using the refueling system to control fusion reactor burn *15th IEEE/NPSS Symp. Fusion Engineering* vol 2 (IEEE) pp 562–4
[4] Plummer D. 1995 Fusion Reactor Control *Proc. 16th IEEE/NPSS Symp. Fusion Engineering* vol 2 (IEEE) pp 1186–9
[5] Mandrekas J. and Stacey W.M. 1991 *Fusion Technol.* **19** 57
[6] Haney S., Perkins L.J., Mandrekas J. and Stacey W.M. 1990 *Fusion Technol.* **18** 606
[7] Hawryluk R.J. *et al* 2015 *Nucl. Fusion* **55** 053001
[8] Evans T.E. and The DIII-D Team 2012 *Plasma Fusion Res.* **7** 2402046
[9] McCool S. *et al* 1990 *Nucl. Fusion* **30** 167
[10] Grosman A. *et al* 1990 *J. Nucl. Mater.* **176–7** 493
[11] Evans T.E. 2006 *Nat. Phys.* **2** 419
[12] Baylor L. *et al* 2007 *Nucl. Fusion* **47** 443
[13] Causey R.A. 2002 *J. Nucl. Mater.* **300** 91
[14] Schuster E., Krstic M. and Tynan G. 2003 *Fusion Sci. Technol.* **43** 18
[15] Boyer M.D. and Schuster E. 2015 *Nucl. Fusion* **55** 083021
[16] Gouge M.J. *et al* 1995 *Fusion Technol.* **28** 1644
[17] Pajares A. and Schuster E. 2017 *Fusion Eng. Des.* **123** 607
[18] Pajares A. and Schuster E. 2017 Nonlinear robust burn control in tokamaks with uncertainties in the fueling lines via Lyapunov redesign *Proc. 2017 American Control Conference* pp 3084–9
[19] Hively L. 1977 *Nucl. Fusion* **17** 873
[20] Stacey W.M. 2010 *Fusion: an Introduction to the Physics and Technology of Magnetic Confinement Fusion* 2nd edn (Weinheim: Wiley)
[21] International Atomic Energy Agency 2001 *Summary of the ITER Final Design Report* (*ITER EDA Documentation Series* vol 22) (Vienna: IAEA)
[22] Khalil H. 2001 *Nonlinear Systems* 3rd edn (Upper Saddle River, NJ: Prentice Hall)